Controls on Erosion in the Western Tarim Basin: Implications for the Uplift of Northwest Tibet and Pamir

Peter D. Clift[1,2], Hongbo Zheng[3], Andrew Carter[4], Philipp Böning[5], Tara Jonell[1], Hannah Schorr[1], Xin Shan[6], Katharina Pahnke[5,] Xiaochun Wei[2] and Tammy Rittenour[7]

1 – Department of Geology and Geophysics, Louisiana State University, Baton Rouge, LA 70803, USA

2 – School of Geography Science, Nanjing Normal University, Nanjing 210023, China

3 - School of Resource, Environment and Earth Science, Yunnan University, Kunming, China

4 – Department of Earth and Planetary Sciences, Birkbeck College, London, WC1E 7HX, United Kingdom

5 – Max Planck Research Group for Marine Isotope Geochemistry, Institute for Chemistry and Biology of the Marine Environment (ICBM), University of Oldenburg, 26129 Oldenburg, Germany

6 – Key Laboratory of Marine Sedimentology and Environmental Geology, First Institute of Oceanography, State Oceanic Administration, Qingdao 266061, Shandong, China

7 – Department of Geology, Utah State University, Logan UT 84322, USA

ABSTRACT

We present here bulk sediment major element chemistry, Nd and Sr isotopes, with detrital apatite fission track (AFT) and U-Pb zircon ages to characterize the provenance of the SW Taklimakan Desert and the three major rivers draining this region. We establish the spatial and temporal controls on erosion and sediment transport in the modern Tibetan rain shadow. The Hotan River drains the North Kunlun Block and is characterized by zircon populations at 160–230 Ma and 370–520 Ma. The Yarkand River shares these grains with the Hotan, but also has a very prominent zircon population at 40–160 Ma, which is common in Karakoram basement, indicating heavy sediment flux from

these ranges to that drainage. This implies a strong control by topographic steepness and precipitation mediated through glaciation on erosion. Our zircon data confirm earlier studies that indicated that the Taklimakan sand is derived from both the Kunlun and Pamir Mountains. AFT ages are younger in the Hotan River than in the Kashgar, which drains the Pamir, and both are younger than in the Transhimalaya and parts of the western edge of the Tibetan Plateau. Exhumation is estimated at ~1000 m/m.y in the North Kunlun, and ~500 m/m.y. in the eastern Pamir, which have been exhuming more slowly than the western ranges in the recent past.

Holocene aggradation terracing was dated using quartz optically stimulated luminescence (OSL) methods and is mostly associated with times of fluctuating climate after 4 ka, with phases of valley filling dated at 2.6, 1.4 and 0.4 ka. The heights and volumes of the terraces show that sediment storage in the mountains is not a significant buffer to sediment transport, in contrast to the more monsoonal Indus system directly to the south. South of the Mazatag Ridge a significant eolian deposit accumulated around 500 years ago, but this has been deflated in more recent times,

Comparison of the modern river data with that previously measured from Cenozoic foreland sedimentary rocks shows that no sediment similar to the modern Yarkand River is seen in the ancient record, which is inferred to be relatively young. Uplift of the North Kunlun had started by ~17 Ma, somewhat after the Pamir and Songpan Garze of NW Tibet, dated before 24 Ma. Sediment from the Kunlun reached the foreland basin between 14 and 11 Ma. North Kunlun exhumation accelerated before 3.7 Ma, likely linked to faster rock uplift.

INTRODUCTION

Sediments eroded from mountain chains can potentially provide a relatively continuous record of how such mountains develop, long after the bedrock sources themselves have been eroded away. These sedimentary records allow us to understand whether feedbacks exist between climate, surface processes and the tectonic evolution of the mountains and provide a key complement to study of the bedrock sources. Climate-tectonic interactions have been investigated in the Himalaya, the Cascades, Taiwan and other regions where precipitation is relatively high and where a link between precipitation and erosion has been established over a variety of timescales (Clift et al., 2008; Dadson et al., 2003; Reiners et al., 2003; Whipple, 2009; Wobus et al., 2003).

Establishing if there is a potential linkage becomes more complicated in regions where rainfall is limited but host significant amounts of deposited sediments. In these cases, other processes, such as rock uplift or seismic shaking, may dominate in controlling erosion (Burbank et al., 2003; Wallis et al., 2016) although this remains unresolved. In this study we address whether solid Earth tectonic forces, precipitation, or topography are controlling the patterns and rates of erosion around the western Tarim Basin (western China). In this area rivers are eroding sediment from the Tian Shan, Pamir, and Kunlun, and delivering this to the central parts of the basin to the north and east (Fig. 1). We target three neighboring river catchments that have contrasting characteristics that allow these factors in controlling erosion to be assessed. One river is more seismically active (Kashgar River), one drains steep, glaciated terrain with more precipitation (Yarkand River), and one is limited to the drier, lower elevated ranges of the northern

Kunlun (Hotan River). Furthermore, changes in bedrock characteristics within the Kashgar and Yarkand Rivers mean that the locus of strongest erosion within those basins can be identified and then related to lateral changes in precipitation, topography and rock uplift.

Compared to the southern side of the Tibetan Plateau, the northern margin is drier and precipitation is believed to be mostly brought by the Westerly Jet from moisture sources as far afield as the Mediterranean but with some input from the South Asian Monsoon (Böthe et al., 2012; Karim and Veizer, 2002). The Tarim Basin is the location of one of the largest deserts in Asia, the Taklimakan Desert, which is a major source of dust into the atmosphere and plays a significant role in modulating global climate on various time scales (Shao et al., 2011; Uno et al., 2009). Constraining its origin is important for both Asian and global climate systems because of its role as a major supplier of aerosols to the atmosphere. We investigated the conclusions of Rittner *et al.* (2016) that the bulk of the desert sediment is coming from the Pamir and the Kunlun Shan, and not sourced from the Tian Shan.

In this study we analyzed sediments from three major rivers feeding the Tarim Basin using a variety of geochemical (major and trace element compositions, Sr and Nd isotope ratios), geochronological (U-Pb zircon dating) and thermochronological (apatite fission track) methods to examine where sediments are derived within each catchment. We do this to understand what processes might be controlling erosion in this relatively dry but tectonically active environment. Each river has its own unique geographic setting, with the Kashgar River draining the eastern Pamir, the Yarkand River draining the northern Karakoram and Kunlun, while the Hotan River receives material mostly from

99 the northern Kunlun alone (Fig. 2). By better understanding what is controlling modern
100 erosion in these rivers we constrain how the ancient stratigraphic record can be used to
101 reconstruct the evolving erosion and uplift of the NW Tibetan Plateau, building on earlier
102 studies of the exposed Cenozoic sequences (Cao et al., 2014; Sun et al., 2016; Zheng et
103 al., 2000; Zheng et al., 2010). Although long understood to be much younger than
104 southern Tibet (Tapponnier, 2002), the uplift history of the northern plateau remains
105 controversial, yet it is agreed that the development of its present high altitude has
106 important impacts on the development of the Asian monsoon system (Kutzbach et al.,
107 1993; Molnar et al., 1993; Tada et al., 2016; Zhang et al., 2015). Better documentation of
108 the uplift history of the northern Tibetan Plateau is required in order to constrain its role
109 in controlling continental climate regimes.

110 We also examine the role of climate in buffering sediment flux over millennial
111 timescales through the storage of sediment in valley fills and its release during episodes
112 of incision and the formation of alluvial terraces downstream. In the monsoon-dominated
113 Himalaya such terracing is driven by changes in precipitation, with more sediment supply
114 and valley filling during wetter times and incision during drier periods (Bookhagen et al.,
115 2006). Here we test to see whether the same relationship holds in a much drier, weakly
116 monsoonal climate.

117

118 **GEOLOGICAL SETTING**

119 **Plate Tectonic Setting**

120 The Tarim Basin represents a relatively stable tectonic block within the otherwise
121 strongly deforming zones of western China and northwest Tibet. Mountain building in

this region is usually interpreted as a direct response to India-Asia collision, starting sometime during the Paleogene. The exact timing remains controversial (Aitchison et al., 2007; Najman et al., 2010), although there is increasing evidence that uplift may have begun much earlier than was originally conceived (Kapp et al., 2005; Wang et al., 2012). The Tarim Basin is surrounded by a number of tectonic blocks, which have been assembled as a result of subduction predating the final India-Asia collision. Many of these blocks were rifted from Gondwana and subsequently accreted to the southern margin of Asia during the late Paleozoic–Mesozoic as a result of closure of the Paleo- and then Neotethys Oceans (Sengor and Natal'in, 1996; Yin and Harrison, 2000).

Mountain uplift has radically changed the topography and style of sedimentation across the area (Tada et al., 2010). From latest Cretaceous to early Paleogene, much of the western Tarim Basin was covered by a shallow sea, part of the Paratethys, an epicontinental sea found across much of central Asia, which began to retreat during the Eocene (Bosboom et al., 2011; Schulz et al., 2005). Shallow marine strata of this age are observed along the southwestern margins of the Tarim Basin where they are overlain by a series of clastic sedimentary rocks apparently eroded from the Kunlun to the south and now deformed into a series of thrust sheets that form the frontal ranges of the Kunlun (Cao et al., 2014; Zheng et al., 2000; Zheng et al., 2010).

Major Tectonic Blocks

Each of the major ranges that contribute sediment to the rivers and Taklimakan Desert discussed here have their own unique history that allows their erosional products to be identified and quantified in a mixed sediment. The Tian Shan and Kunlun are

144 formed as a result of crustal thickening, with some localized strike-slip faulting (Avouac
145 and Tapponnier, 1993). Sobel and Dumitru (1997) argued that thrusting became the
146 dominant mode of deformation by ~25–20 Ma across the region, spanning the Pamir and
147 Kunlun to the Tian Shan. The Pamir form a large, arcuate, north-propagating mountain
148 belt that represents the along-strike equivalent of units found in the Karakoram and
149 Western Tibet (Robinson et al., 2004). This range is particularly well-known as an
150 example of ongoing continental subduction of Asian lithosphere towards the south under
151 the Indian plate (Burtman and Molnar, 1993) and may represent a younger tectonic
152 process not directly linked to initial India-Asia collision. The northern Pamir have been
153 interpreted as a composite Paleozoic arc terrane correlative to the North and South
154 Kunlun Terranes of the western Kunlun Shan (Fig. 2)(Boulin, 1988; Kapp et al., 2007;
155 Tapponnier et al., 1981; Yin and Harrison, 2000). Nonetheless, direct correlation between
156 the Pamir and Tibetan Plateau is still controversial. The Pamir differ from the Himalaya
157 and Tibet in the relative abundance of metamorphic domes that are especially common in
158 the western Pamir, but are also found to a lesser extent in the western parts of our field
159 area in the Kunlun south of Kashgar (Burtman and Molnar, 1993; Robinson et al., 2012).
160 The Pamir domes are larger than those documented in Tibet and are dated as Cenozoic in
161 their exhumation, which was especially rapid during the Miocene (Hubbard et al., 1999;
162 Robinson et al., 2007).

163 The Karakoram represent a complicated tectonic block composed of Mesozoic-
164 Cenozoic metamorphic rocks, as well as limited amounts of sedimentary rocks (Searle,
165 1991), together with a large Miocene batholith that intrudes the sequence and is
166 associated with post-India-Eurasia collisional melting (Searle et al., 1989). The early

magmatic history of the Karakoram involves Cretaceous intrusive rocks related to an active continental margin along the southern margin of Asia (Searle et al., 1990), possibly equivalent to the Gangdese Batholith in central south Tibet. The Karakoram is cut by a major strike slip fault whose timing and degree of motion has been controversial (Murphy et al., 2000; Peltzer and Tapponnier, 1988; Phillips et al., 2004). However, it is clear that this structure is right-lateral and documented to drive rapid rock uplift and exhumation in central parts of the Karakoram to present day (Foster et al., 1994; Searle and Phillips, 2007), which form the southern edge of the Yarkand catchment.

METHODOLOGY

Each of the tectonic blocks mentioned above has its own unique geological history, which we can exploit to trace from where the sediments in the modern rivers are derived. The wide variety of rock compositions of different ages from each tectonic block (Fig. 3) produce mineral phases that contain unique chemistry and ages. When we analyze these in the modern river sediments we have the chance to constrain the relative contribution that each block makes to the total sediment flux for each particular river. In doing so we can isolate regions producing the most sediment and thus determine what processes might control our observed rates of erosion.

We choose to employ bulk sediment Sr and Nd isotopes to determine the overall provenance of the sediment. Nd is a robust provenance proxy because this element is generally immobile during weathering and erosion (Goldstein et al., 1984). Furthermore, recent work has shown that the Nd content of sediment is largely controlled by the Nd-

189 bearing phases monazite and allanite that are not separated by density-related mineral
190 sorting during transport and so can be considered immune to hydrodynamic processes
191 (Garçon et al., 2013; Garçon et al., 2014). In contrast, Sr isotopes may be more
192 susceptible to change during transport and are also affected by chemical weathering and
193 the presence of carbonate (Derry and France-Lanord, 1996). These caveats make Sr
194 isotope compositions a less reliable provenance tool, but when used in combination with
195 Nd isotopes can be effective. In addition, we use bulk sediment major element
196 compositions to quantify the degree of chemical alteration as an independent technique to
197 assess Sr isotope values and, to a lesser degree, sediment provenance.

198 Our analysis hinges on thermochronology of single detrital grains because these
199 can identify and quantify individual end member sources that are obscured in the bulk
200 analysis. Detrital zircon U-Pb dating has become a popular and effective technique for
201 evaluating sediment provenance in clastic systems because zircon is a common mineral in
202 continental rocks, and is chemically and mechanically durable enough to survive multiple
203 cycles of erosion, transport and sedimentation (Gehrels, 2014). Spot size of the laser
204 employed limited analysis to grains >50 μm across. Yang *et al.* (2012) demonstrated that
205 younger zircons were larger and/or more variable in size than older zircons in the
206 Yangtze River, indicating a potential influence of transport on zircon size and age.
207 Nonetheless, these authors concluded that the 63–125 μm size fraction yielded almost the
208 same age distribution as the total zircon population, and accurately represents all
209 significant age populations. Our analysis of the 63–125 μm fraction is thus representative
210 of the bulk composition. Given that the rivers examined here are so much shorter than the
211 Yangtze (~170 km between the headwaters and the sample point in the Kashgar, ~450 km

in the Yarkand, and ~150 km in the Hotan), grain size effects would be less significant, because there would be less abrasion of zircon during shorter transport.

We also employ apatite fission track thermochronology of detrital grains, when apatite was present in sufficient quantities, as a provenance proxy and to constrain rates of exhumation in the source regions. The low-temperature apatite fission track method records cooling through ~60–125°C over timescales of 1–10 m.y. (Green, 1989), so is particularly sensitive to exhumation driven by erosion and has been widely used in exhumation studies worldwide, including northern Tibet (Duvall et al., 2012; Jolivet et al., 2001), Pamir (Lukens et al., 2012; Sobel et al., 2006a; Sobel et al., 2006b) and the Tian Shan (Sobel and Dumitru, 1997; Tang et al., 2015).

We also attempt to examine how Quaternary climate change may have impacted sediment transport and to do this we sample fluvial terraces found within the valleys feeding the south side of the Tarim Basin, as well as from selected aeolian deposits within the Tarim Basin itself. Age control for Holocene deposits was determined using optically stimulated luminescence (OSL) dating of quartz in sediments. This technique dates the last time the sediment was exposed to sunlight, presumably during transport. It is widely applied to quartz-bearing sediment, largely deposited in the past 200 k.y. (Rhodes, 2011).

SAMPLING

Samples were taken for provenance and OSL dating from along the SW edge of the Tarim Basin. Sample locations are shown in Figure 1 and are listed in Table 1.

Sediments containing fine to medium sand (>63 μm) were preferentially sampled for provenance analysis. This size fraction is ideal for single-grain mineral provenance techniques that are limited by an analytical laser spot size >50 μm. We recognize that by only analyzing the >63 μm sediment we are not including the suspended load which may have a different provenance and could introduce bias to the bulk sediment provenance interpretation (Garzanti et al., 2011). However, our data are derived from a wide array of grain-sizes >63 μm, which we argue contribute to an initial constraint on sediment generation patterns in this region.

Three proximal river sands from the Kashgar (13062701), Yarkand (13062101) and Hotan (13062401) rivers were sampled near where they leave their mountain source areas to quantify the sediment being produced in the ranges and before any significant recycling of older sediment within the flood plains were to be incorporated. The Hotan was sampled from its larger, western Kalakash branch. These samples were chosen because the Kashgar River is the largest river draining ~11,000 km^2 of the Pamir into the Tarim Basin, while the Hotan River allows us to assess the erosion flux from ~12,500 km^2 of the North Kunlun (Fig. 2). In contrast, the Yarkand drains ~25,000 km^2 as far south as the Karakoram and permits us to quantify what their contribution has been to sediment flux into the Tarim Basin. Samples were taken directly from the banks of the active stream where the sediment had clearly been recently transported.

Sample 13062403 was taken from the Hotan River in the center of the Tarim Basin to assess how much recycling of sediment from the Taklimakan Desert into the river had occurred and to what extent the erosional signal from the upper Hotan is propagated into the basin. Sample 13062402 was taken from a dune within a major sand

sea in the central part of the basin, south of the Mazatag Ridge (Fig. 1) in order to characterize the origin of the sediment in that part of the desert and test the proposed dominant provenance in Pamir and the Kunlun Shan (Rittner et al., 2016). Although eolian sand may have experienced more reworking that the more proximal fluvial sediments it is still possible to assess provenance using the same methods.

Samples for OSL dating were taken from two regions. South of the Mazatag Ridge there are a series of prominent sediment mounds with Euphrates poplar trees growing on their summits (Figs. 4A and 4B). Wind-blown silt and sand under these trees are fixed and buffered from transport by well-established root systems. These sediment mounds overlie older meandering river sediment, which suggests this area clearly was a region of net deposition for desert sediments. However, in more recent times the region has been significantly deflated, leaving only the remnants of the poplar mounds. Sand continues to accumulate on the north side of the Mazatag Ridge (Fig. 4F), implying a change in wind dynamics. Our samples were designed to date the age of accumulation and place a lower boundary on the time of the wind reorganization and deflation.

Aggradational fill terraces along the upper Kargilik River, a tributary to the Yarkand (Fig. 1), were also sampled for OSL dating. Although the Kargilik is not the main stream of the Yarkand it appears that such terraces are of regional extent and representative of the geomorphology. These terraces rise >15 m above the modern river bed, with at least two lower terrace levels identified in the valley (Figs. 4C and D). Although these terraces are now farmed there is little agricultural disturbance upstream. We sampled here to date times of net valley aggradation and to place a lower bound on the incisional episodes. In addition, we sampled a 4 m high Kesile River terrace (Sample

13062703) immediately west of Kashgar to establish whether timing of aggradation and incision were regionally synchronous between the Pamir and the Kunlun River basins.

ANALYTICAL METHODS

Details regarding geochemical, provenance, and OSL analyses are provided in the associated Supplementary Information file and are summarized here. Samples were analyzed for major and trace elements to provide a basic characterization of the material by X-Ray Fluorescence (XRF), with data presented in Table 2. Sediments were also analyzed for Sr and Nd isotopes because these systems have an established track record of being reliable provenance and chemical weathering proxies in sedimentary systems (Goldstein et al., 1984). The isotopic compositions of Nd and Sr were analyzed on a Thermo Neptune Plus Multicollector ICP-MS at the ICBM, Oldenburg, Germany. Isotopic results are reported in Table 2. Nd isotope analyses were corrected against JNdi-1 standard. We calculate the parameter ε_{Nd} (DePaolo and Wasserburg, 1976) using a $^{143}Nd/^{144}Nd$ value of 0.512638 for the Chondritic Uniform Reservoir (CHUR (Jacobsen and Wasserburg, 1980)).

Detrital zircons were dated using the U-Pb method at the London Geochronology Centre facilities at University College London (UK), using a New Wave Nd:YAG 193 nm laser ablation system, coupled to an Agilent 7700 quadrupole ICP-MS. Around 100–120 grains are considered generally sufficient for characterizing sand eroded from a geologically complicated drainage basin (Vermeesch, 2004). Results are presented in Table S1.

Depositional ages of sediment in the terraces were determined by OSL dating of quartz sand following the single-aliquot regenerative dose method (Murray and Wintle, 2000). While OSL dating can be challenging in fluvial environments, deposits from these settings can be accurately dated by selecting depositional facies most likely to have been reset by sunlight exposure (Fuchs and Owen, 2008; Rittenour, 2008; Wyshnytzky et al., 2015). We preferentially targeted well-sorted, horizontally bedded sand lenses from fluvial deposits to reduce the influence of incomplete resetting (partial bleaching) of the luminescence signal. Samples were processed at the Utah State University Luminescence Laboratory and results are presented in Table 3. More information on sample processing, analysis and equivalent dose distributions can be found in the Supplementary Information.

RESULTS

Mineralogy

Samples were predominantly quartz-rich, well-sorted, and sub-angular to sub-rounded sands (Fig. S1). It is noteworthy that the desert dune sand, sample 13062503 (Fig. S1D) does not show a particularly rounded morphology, indicating that these sediments may not have been recycled within the desert for a long time. However, this sample is richer in quartz compared to other analyzed sands. There is a significant minority population of mafic heavy minerals and lithic fragments, particularly metamorphic rock fragments in all samples, that dominate compared to volcanic lithic grains, although carbonate grains are also present, except in the Hotan River (13062401). Quartz tends to be monocrystalline, although with a significant subpopulation of polycrystalline, metamorphic quartz. The sample from the Kashgar River (13062701) is

noteworthy in having a particularly high proportion of chert fragments. When plotted on the QFL diagram of Ingersoll *et al.* (1984) the sands plot within the recycled orogenic field (Fig. 5A).

Bulk Sediment Chemistry

Bulk sediment chemistry reveals a relatively normal, quartz-rich continental sand composition for all samples. On the A-CN-K plot of Fedo *et al.* (1995) the samples plot towards the CN axis and show very low Chemical Index of Alteration (CIA) values using the equation of Nesbitt *et al.* (1980)(Fig. 5B). This indicates that the sediments are very weakly altered compared to their bedrock source, despite their apparent recycled orogenic assignment. Radiogenic isotopes show a limited range in Nd isotope composition, with ε_{Nd} values spanning -8.1 to -9.9, while $^{87}Sr/^{86}Sr$ values are quite widely dispersed between 0.71171 (Kashgar River) and 0.72195 (Upper Hotan)(Fig. 6).

Apatite Fission Track

Because of insufficient apatite only three samples could be analyzed for apatite fission track to constrain both provenance and regional exhumation rates. The analyses were performed at University College, London (UK) with the results presented in Table S2 and Figure 7. The Hotan River sample shows a dominant young age peak at 3.7 ± 0.4 Ma, with a central age of just 9.9 Ma. Two other peaks are noted at 17.3 and 107 Ma, but these are much less abundant. The lower Hotan sample yielded a less well defined but similar age spectrum, with a central age of 28 ± 7.4 Ma and a prominent younger population detected at 5.3 ± 0.9 Ma. The dune sand has the oldest fission track ages with

346 a central age of 37.3 ± 7.5 Ma and a prominent peak of 8.1 ± 0.9 Ma, as well as two older
347 populations clustered at 30.8 and 178 Ma.

348 **U-Pb Zircon Dating**

349 Four of the five sand samples yielded >110 grains for U-Pb dating, which is
350 generally considered to be the threshold for an accurate statistical representation for a
351 sediment derived from a complex source terrain (Vermeesch, 2004). Only the Yarkand
352 sample had significantly less than this number (43), and so our inferences based on those
353 data must be considered less reliable. The age spectra for the samples are shown in Figure
354 8. We identify six prominent age populations that are common to many of the samples,
355 40–160 Ma, 160–230 Ma, 230–370 Ma, 370–520 Ma, 520–690 Ma, 690–900 Ma and
356 >900 Ma. There are very few grains older than 900 Ma, or younger than 40 Ma. The
357 Yarkand River is distinctive in showing a prominent population at 40–160 Ma that is not
358 found in the other rivers. In contrast, the Upper Hotan is unique in having a very
359 abundant 160–230 Ma population, although this group is also seen at lower
360 concentrations in the dune sand and the lower Hotan sample. The Kashgar River has
361 prominent populations at 370–520 Ma and 520–690 Ma and is unique in our dataset in
362 having a sizable 690–900 Ma population (Fig. 8). The dune sand and lower Hotan
363 samples have relatively similar age spectra, although the dune sand has a more abundant
364 230–370 Ma population.

365 **Optically Stimulated Luminesence**

366 The OSL ages reveal a relatively young set of terraces along the Kargilik River
367 with the oldest dating to 2.57 ± 0.46 ka and two younger lower terraces at 1.40 ± 0.46 ka

and 0.42 ± 0.19 ka respectively (Table 3). Other young ages of sedimentation are found in the Mazatag Mounds that represent deflated remnants of desert dunes on the south side of that range. Depositional ages here are only 0.50 ± 0.20 ka. Finally the terrace above the Kashgar River near Kashgar provides a depositional age of 2.76 ± 1.24 ka, close to the older terrace age in the Kargilik valley.

DISCUSSION

Sediment Provenance

Bulk Isotope Chemistry

We now use the data presented above to make inferences about the source of sediment in the modern river systems by comparing new data presented here with existing bedrock data. Figure 6 shows that the Hotan River (13062401) has a Sr and Nd isotope composition that lies within the range of bedrock and proximal moraine compositions from the Kunlun, albeit with higher than average $^{87}Sr/^{86}Sr$ values. This relationship might be expected based on the modern drainage pattern of that river (Fig. 2). In contrast, the Yarkand River (13062101) plots at a similar ε_{Nd} value but lower $^{87}Sr/^{86}Sr$ value, within the range of the Karakoram basement, as well as being close to basement of the Tianshuihai Massif. The tectonic zonation map (Fig. 2) indicates that the Tianshuihai Massif is composed of both Karakoram and Songpan Garze terranes. The Sr and Nd data suggest that most of the sediment in the Yarkand is being derived from its upper reaches and not from the northern parts of the catchment closer to the edge of the Tarim Basin itself. The Kashgar River (13062701) plots at a lower $^{87}Sr/^{86}Sr$ value again, closer but

still above the range of the various volcanic suites of the Ashikule Volcanic Group. The rocks of the Tuyon Basin lie within the Kashgar drainage, but have much lower $^{87}Sr/^{86}Sr$ values and higher ε_{Nd} values, indicating that any erosion from those rocks is quite limited. Instead erosion appears to be dominated by sources isotopically similar to those supplying the Yarkand River. Not surprisingly, the Lower Hotan (13062403) and the dune sand (13062503) plot close together, consistent with significant reworking of desert sand into the river. The desert sand itself is intermediate between the Hotan and Yarkand samples in Sr and Nd, and has higher $^{87}Sr/^{86}Sr$ values than earlier analyses from the Taklimakan Desert (Chang et al., 2000). Our desert sand data could be explained by erosion from a mixture of Kunlun and Pamir (Kashgar) sources, consistent with the findings of Yang *et al*. (2007) and Rittner *et al.* (2016). Our sediment appears to show more Kunlun and less Pamir influence compared to the earlier analyses that were taken along the northern edge of the Tarim Basin. Our Nd and Sr data do permit the possibility that the Karakoram have been a source to the desert, although this is not required.

Zircon U-Pb Evidence

We can explore these conclusions further by consideration of the zircon U-Pb ages. The Hotan River is marked by a very prominent population at 160–230 Ma (Fig. 8). This population is not commonly found in the other rivers and given the extent of the drainage must be derived from the Kunlun, likely the North Kunlun terrane (Fig. 2). Although basement samples from this area have not yet shown this peak, this implies inadequate sampling of the basement to date. It is noteworthy that this 160–230 Ma group , although as yet unseen in bedrock analyses, exists as a very prominent population within Cenozoic sedimentary rocks preserved within the Kunlun (Bershaw et al., 2012).

The Yarkand River shares with the Hotan River zircon age populations at 160–230, and 370–520 Ma, which is unsurprising given that this river also drains through the South and North Kunlun. However, the Yarkand contains a very prominent peak at 40–160 Ma, which is not seen in the other rivers but is common in Karakoram basement. This indicates that a large quantity of the sediment in the Yarkand River is derived from the Karakoram, consistent with bulk isotope data and the modern drainage geometry.

The Kashgar River differs from the other rivers in showing a significant 230–370 Ma group, as well as an older 690–900 Ma population, almost unknown in the other rivers, or the Taklimakan Desert. The Kashgar River shares the strong 370–520 Ma group with the other studied rivers. This group is well known from basement samples in the Kunlun, which forms the southern side of that drainage, implying erosion from that region. The differences in the observed zircon ages and age frequencies between the Kashgar and Hotan Rivers would thus likely reflect the influence of sources to the north, within the Tian Shan. As with the bulk isotope data, the downstream Hotan River and the dune sands share a similar pattern in U-Pb zircon ages. These two samples also share several populations with the upstream Hotan and Kashgar Rivers, but not with the Yarkand, implying that this river is not a major source of sediment to the Taklimakan Desert. This may indicate that the flux from the Yarkand is overwhelmed within the Tarim Basin by flux from other rivers, and/or that drainage from the Karakoram to the Tarim Basin has initiated quite recently. Our zircon data are consistent with the work of Rittner *et al.* (2016) in demonstrating that the Taklimakan dune sand reflects input from both the Kunlun and Pamir.

Controls on Provenance

What controls the rates of erosion between the different river basins remains problematic because we do not have information on the volumes of material sourced by the Kashgar, Yarkand and Hotan Rivers. The Kashgar River catchment is easily the most tectonically active (Fig. 1) but is otherwise unremarkable in terms of its topography or precipitation (Fig. 9). The Kashgar appears to be steeper and slightly wetter on its northern side compared to its southern side. Provenance constraints from U-Pb detrital zircons indicates that more sediment is being derived from north of the drainage (Fig. 6), raising both these factors as possible crucial constraints. The Yarkand River drains the steepest topography, especially in its headwaters close to the Karakoram, where it also experiences relatively high rates of precipitation. The combination of steep local topographic relief and precipitation, that encourages strong glacial development, may be the reason that this part of the catchment is so productive relative to the Kunlun. In contrast, the Hotan River is the driest catchment with only slightly higher rates of precipitation in its western reaches. It is also the most topographically reduced. However, because the Hotan River drains essentially only one major tectonic block our data does not allow us to resolve what is controlling the distribution of erosion patterns within this drainage. In the other cases however, there is a consistent link to climate, and especially precipitation, being the primary control over relative erosion rates within a given basin, even if tectonics is forming the topography against which orographic precipitation is occurring.

Paleo-Erosion Patterns

We apply our understanding of the erosion in the modern rivers to interpretation of ancient deposits to better constrain the erosion of the northern edge of the Tibetan

459 plateau. Cao *et al.* (2014) published a series of detrital zircon U-Pb ages from a section
460 close to the modern Hotan River and used these to reconstruct the progressive
461 exhumation of the northern edge of the Tibetan Plateau during the Cenozoic. In our
462 reassessment we assign depositional ages based on the stratigraphic correlation shown in
463 Figure 10 and using the revised ages from Zheng *et al.* (2015), who employed a slightly
464 different lithostratigraphy. The age of the base of the section is well defined as Eocene,
465 based on marine fossils, while the top of the section, defined as the Xiyu Formation by
466 Zheng *et al.* (2015) is dated at 11 Ma based on a volcanic ash deposit. We correlate these
467 two sections with the revised depositional ages to aid in our understanding evolving
468 erosion patterns.

469 The oldest formation, the Keziluoyi, yielded strong zircon age peaks at ~300 and
470 450 Ma (Fig. 11), that are also observed in the Kashgar River, as well as in the desert
471 sands. However, the Keziluoyi Formation lacks the 690–900 Ma population found in the
472 Kashgar River. It seems likely that the Keziluoyi Formation had similar sources to those
473 now supplying the desert sand, implying erosion both from the Pamir and from the
474 Kunlun.

475 We employ multidimensional scaling (MDS) (Fig. 12) to assess the similarity of
476 ancient and modern sediments and their potential bedrock source terranes (Vermeesch,
477 2013). MDS is a standard statistical technique similar to Principle Component Analysis,
478 with can be used to create a plot measuring the similarity between sample zircon age
479 spectra much like the Kolmogorov-Smirnov method that quantifies the distance between
480 the empirical cumulative distribution functions of two samples. MDS plot axes are
481 themselves are not physical parameters.

The Kolmogorov–Smirnov statistic quantifies a distance between the empirical distribution functions of two samples. Like the desert sand the Keziluoyi plots between the Pamir-derived Kashgar and the upper Hotan Rivers. This implies that at least some parts of the northern plateau and Pamir were already exposed between 24 and 30 Ma.

The overlying Anjuan Formation shows a strong provenance change, with a sharp increase in grains <100 Ma, as well as the appearance of a significant 690–900 Ma population. New sources must have been exposed by that time (24 to <18 Ma) and this older zircon population indicates that these may be derived from the Pamir. This indicates an established river drainage from that area must have been established and delivering (significant?) sediment to the southern edge of the Tarim Basin at that time, i.e. the Early Miocene. Although Cao *et al.* (2014) argued that the young (<40 Ma) grains were coming to the Anjuan Formation from the Karakoram via a paleo-Yarkand River we prefer a source in the western Pamir, based on the closer overall similarity of the U-Pb spectra (Fig. 12) and lack of ~60 Ma grains in the Anjuan Formation that are common in the Karakoram (Fig. 8), but absent in the West Pamir and the Anjuan Formation, at least at the 95% confidence level. We think a drainage connection with the Karakoram at that time unlikely and we can conclude with confidence that if such a link did exist then the amount of sediment supplied was very limited. The MDS diagram indicates that the Anjuan Formation has similarity with basement sources in the Cretaceous sedimentary rocks of the Kunlun, as well as in the Songpan Garze (Fig. 12). This implies erosion, sediment delivery from, and thus possible uplift in the Kunlun, in addition to that seen in the Pamir at the time of sedimentation. This interpretation is in accord with the AFT data from the Hotan River. The western Pamir no longer supply sediment to the Tarim Basin

505 so some drainage reorganization is required between the west and east Pamir since the
506 Early Miocene.

507 The overlying Pakabulake Formation (~14 Ma) is characterized by the
508 disappearance of zircon populations <100 Ma, and 230–370 Ma, and another sharp
509 decrease in the relative influence of 690–900 Ma zircons. The source of the Pakabulake
510 Formation would appear to be mostly within the Kunlun and northern Tibetan Plateau,
511 without significant sediment influx from the Pamir. Such a switch is probably at least
512 partly linked to drainage capture away from the area of sedimentation rather than because
513 the Pamir were not eroding. Comparison between the Pakabulake and overlying Artux
514 Formations shows a significant provenance change between from 14 to 11 Ma,
515 particularly with the appearance of a very strong 160–230 Ma population. This is
516 identical to that seen in the modern Hotan River, and which we know to be derived from
517 the north Kunlun terrain. As a result we infer the start of sediment flux from the North
518 Kunlun Block to the region of the measured sections between 14 and 11 Ma, with the
519 implication that earlier erosion from the Kunlun must have been from the South Kunlun,
520 or even potentially from the Songpan Garze. The appearance of North Kunlun material
521 between 14 and 11 Ma is later than the start of exhumation implied by the ~17 Ma AFT
522 in the Hotan River. This lag may reflect drainage reorganization, with Kunlun sediment
523 being deposited elsewhere between 17 and 11 Ma.

524 A regional evolution model for the foreland sequence is one of uplift propagating
525 from south to north during the Early-Middle Miocene with most of the ranges we now see
526 presently in existence by around 11 Ma. This is slightly earlier than the Mid-Late
527 Miocene uplift implied by Cao *et al.* (2014) and Wang *et al.* (2003). It is also noteworthy

528 that no sediment similar to the modern Yarkand River is seen in the ancient record,
529 suggesting that this river system is relatively young and that the connection between
530 drainage systems sourcing Karakoram material into the Tarim Basin is a relatively recent
531 development. This is consistent with the observation that grains <100 Ma are not found in
532 Taklimakan Desert sands that implies minimal delivery from such sources in the
533 geological past.

534 **Regional Exhumation from Fission Track**

535 Apatite fission track (AFT) data can be used to look at regional exhumation rates
536 within the drainage of the Hotan River and the sources to the Taklimakan Desert. If we
537 assume a standard range of continental geothermal gradients of 25–30˚C/km and a simple
538 cooling history then we can use the age population of the sands to estimate average
539 exhumation rates in the sources. The dominant population in the Hotan River clusters at
540 3.7 ± 0.4 Ma, which implies exhumation rates of 894–1333 m/m.y. if the base of the
541 partial annealing zone is placed at 110˚C (Green, 1989). Our reported central age for the
542 Hotan River is comparable to those reported from the Eastern Karakoram at 3.3 ± 0.3 Ma
543 and 7.4 ± 1.1 Ma (Wallis et al., 2016), but is older than those from the Central Karakoram
544 around K2 (Foster et al., 1994). Our AFT ages are much younger, and thus exhumation is
545 calculated to be much faster, than in the Transhimalaya and SW edge of the Tibetan
546 Plateau (Dortch et al., 2011; Kirstein et al., 2006; Munack et al., 2014).

547 This exhumation rate should reflect the average exhumation rate of North Kunlun
548 bedrock sources that we identified above as the primary supplier to the Hotan River.
549 Although there are two older AFT populations these are numerically much smaller and do

not dominate the sediment flux. Together our detrital zircon and AFT data indicate that there has been rapid exhumation of at least parts of the North Kunlun, since at least 3.7 Ma. However, we also note that there have been moderate rates of exhumation in parts of the Kunlun since ~17.3 Ma (185–297 m/m.y.), consistent with basement AFT work (Sobel and Dumitru, 1997), but which occurred still much faster than long term rates dating back to the Cretaceous. These older AFT ages are not so common but do indicate significant regional unroofing back into the Mid Miocene. If these cooling events were triggered by rock uplift then we could infer that uplift of the North Kunlun initiated by ~17 Ma and accelerated no later than 3.7 Ma. The later acceleration is consistent with tilting and facies changes seen in the Mid-Late Miocene Xiyu Formation of this area that suggests major uplift starting after ~15 Ma (Wang et al., 2003; Zheng et al., 2000).

The AFT ages in the Tarim sands are also dominated by younger ages at ~8.1 ± 0.9 Ma, albeit slightly older than those in the Hotan River. This indicates that the average source of the Tarim dunes is exhuming a little more slowly than the Kunlun sources of the Hotan River. The combined zircon and Nd-Sr isotope data indicate that the desert sands are from both the Kunlun and Pamir, which implies that the Pamir sources are exhuming more slowly than the Kunlun in the recent past. Average exhumation rates of the dominant dune sand population (~8.1 Ma) are around 407–611 m/m.y. and 105–165 m/m.y. for the fission track ages clustered at ~30.8 Ma, if we consider both the uncertainty in the geothermal gradient and the uncertainty in the AFT population ages. Despite the uncertainties exhumation rates of the average dunes, and thus the eastern Pamir, are slower than those seen in the Kunlun.

572 We can also compare these rates with regional exhumation in the west Pamir
573 published by Lukens *et al.* (2012). That study did not include AFT data but $^{39}Ar/^{40}Ar$
574 mica dating yielded a young population there of 13–21 Ma. If we use a closure
575 temperature range of 350–420˚C (McDougall and Harrison, 1999) for the mica and our
576 geothermal gradient range of 25–30˚C/km then we can estimate average exhumation rates
577 of up to 1300 m/m.y. and as low as 560 m/m.y. in the western Pamir. This range is higher
578 than the 407–611 m/m.y. range estimated from the Tarim sands, indicating that the
579 eastern Pamir has been exhuming less rapidly than the western ranges. Furthermore, we
580 note that although Lukens *et al.* (2012) emphasize that the Pamir are exhuming faster
581 than western Tibet, our data from the Hotan River indicates that at least the North Kunlun
582 are exhuming at comparable rates, i.e., ~894–1333 m/m.y. at least during the Plio-
583 Pleistocene.

584 **Holocene Sediment Transport**

585 Examination of the alluvial terraces in the rivers draining the Kunlun yield a
586 series of rather young valley-filling ages with no clear evidence for other higher and older
587 terraces in the same valleys. In the Kargilik River we see evidence for aggradation at
588 around 2.6, 1.4 and 0.4 ka. We find that in each case the height of the terrace is neither
589 especially high (<15 m) nor the along-stream extent very great. This suggests that
590 sediment storage within the mountains is not an important factor in buffering the total
591 sediment flux from the mountain sources to the depocenter. A regional climatic trigger
592 for valley aggradation and incision would explain the relative coincidence of terrace ages
593 in the Kargilik and Kashgar Rivers at ~2.5 ka. In the more monsoonal sectors of the
594 Himalaya, valley aggradation is usually associated with an increased sediment supply

595 driven by a strong monsoon (Bookhagen et al., 2006). In this more northern area the
596 monsoon has less influence and moisture is largely supplied via the Westerlies. This is
597 likely one of the reasons that the strong aggradation recorded in the Himalaya over the
598 early Holocene (10–8 ka) is not observed in this region. Climate records from western
599 China are reflective of a complicated history, although some would argue for a dry and
600 warm phase between 11 and ~7 ka followed by warm and wet phase between 7 and 4 ka,
601 and that followed in turn by a fluctuating cool and dry period (Feng et al., 2006).
602 However, such syntheses cover very wide areas with regional differences between
603 Kunlun and Tianshan being lost.

604 A typical view is that the Tarim Basin experienced a Holocene climatic optimum
605 between 8 and ~5 ka that is not so different from the situation in the western Himalaya
606 (Dixit et al., 2014; Wünnemann et al., 2010). However, there is a lack of agreement on
607 the climatic evolution in western China. A study by Hartmann and Wünnemann (2009)
608 from a lake deposit from north of the Tarim Basin argues for an episode of dry conditions
609 between 7.5 and 5.4 ka. This is followed by greater runoff and wetter conditions after 5.4
610 ka, with the final phase of drying after 4.0 ka. This lake record seems to indicate an
611 extremely variable monsoon within NW China over the Holocene as a result of
612 interactions between the Indian summer monsoon and the winter Westerly Jet.
613 Observations in the recent historical past indicate that the Asian summer monsoon is
614 typically responsible for extreme rainfall events that are more likely to result in sediment
615 transport in the Tarim Basin (Yatagai and Yasunari, 1998). Over the Holocene, Holmes *et*
616 *al.* (2009) summarized proxy data from ice cores, tree rings, and lacustrine sediments that
617 confirmed both significant variability in climate across the region and with altitude. Lake

618 records from this area study compiled by Wünnemann *et al.* (2006) were able to identify
619 times of significant desiccation, which they were able to date in the more recent past
620 between 2.6–2.5, 1.9–1.1 and 0.5–0.3 ka, close to the ages of our terrace sediments from
621 the Kargilik River.

622 Given the age uncertainties in the OSL dating (Table 3) it is not clear whether the
623 valley aggradation was associated with wet periods or the drier intervals because both
624 intervals were quite short-lived. It is presumed that aggradation is related to increased
625 sediment supply during wetter periods. Terracing is mostly associated the time of
626 fluctuating climate after 4 ka. Nonetheless, the height and volume of the terraces make it
627 clear that sediment storage in the mountains is not a significant buffer to sediment
628 transport, in stark contrast to the extensive terraces in the Indus River system (Blöthe and
629 Korup, 2013; Clift and Giosan, 2014). In contrast to river systems in more monsoonal
630 areas there is no suggestion that historic anthropogenic impacts via agricultural disruption
631 has triggered intensified upstream erosion resulting in downstream valley aggradation
632 (Jonell et al., 2016).

633 Within the Taklimakan Desert itself there are clearly short-term changes in the
634 accretion and deflation of dune complexes. South of the Mazatag Ridge a significant
635 eolian deposit accumulated around 0.5 ka, but this has been deflated in more recent times.
636 This period coincides with the dry period noted by Wünnemann *et al.* (2006). It is
637 possible that the shift from drier to wet conditions estimated at ~0.3 ka may be linked to
638 reorganization of regional winds, which resulted in the change from sediment accretion to
639 erosion in that area. Although the Taklimakan Desert has the potential to be a major
640 sediment buffer over longer timescales, the Holocene record we observe and that is

reported in the existing literature indicates rapid sediment recycling over millennial time scales.

CONCLUSIONS

Combined radiogenic isotopes and U-Pb dating of detrital zircons from three rivers in the western Tarim Basin reveal the nature of the source terranes, the origin of the sediment in these rivers, as well as those in the dune fields of the Taklimakan Desert. The Yarkand, Hotan and Kashgar Rivers all show unique provenance signatures. The Yarkand derives much of its sediment from steep, glaciated terrains, largely sourced from the Karakoram near the north flank of K2. This river appears to be relatively new because no sediments with similar U-Pb zircons ages are found within Cenozoic foreland basin strata from at least ~11 Ma. Zircon grains <100 Ma are essentially nonexistent in the Taklimakan Desert sands and so imply a low net supply from the Karakoram via a paleo-Yarkand River. A combination of U-Pb zircon and isotope data confirm earlier studies that desert sands are derived largely from a mixture of Kunlun and Pamir sources (Rittner et al., 2016).

The Hotan River derives most of its material from the North Kunlun and shows a population of grains dated at 160–230 Ma that has not yet been discovered in the bedrock of that tectonic block. The Kashgar River appears to be deriving sediment from both northern and southern flanks of that catchment, although with greater flux from the Tian Shan than from the Pamir. As in the Yarkand, this implies that precipitation is the key

process controlling erosion in each river basin, although this is sometimes reinforced by tectonically generated topographic processes.

Apatite fission track data from Hotan River and desert dunes indicate rapid exhumation of the North Kunlun since 3.7 Ma following a period of more moderate, but still significant exhumation in the middle Miocene, at least by ~17 Ma. These rates of exhumation are comparable to those found in the eastern Karakoram (Wallis et al., 2016), and are faster than much of the Transhimalaya and western Tibet (Dortch et al., 2011; Kirstein et al., 2006; Munack et al., 2014) but slower than those seen in the central Karakoram (Foster et al., 1994). Apatite fission track-derived exhumation rates show that the Eastern Pamir have been exhuming more slowly than the western Pamir. Examination of the Cenozoic foreland strata reveals a pattern that suggests a northward propagation in uplift and exhumation that is not clearly linked to climatic evolution. The oldest sediments of the Keziluoyi Formation, (24–30 Ma) are derived from the Pamir and partly from northern Tibet (Songpan Garze). The subsequent Anjuan Formation, which is younger than 18 Ma, shows erosion from the western Pamir but not the Karakoram as previously believed (Cao et al., 2014), as well as influxes from an uplifting Kunlun Block. The overlying Pakabulake Formation (~15 Ma) shows a loss of drainage from the Pamir, suggesting drainage reorganization possibly linked to headwater transfer from the eastern to western Pamir Rivers and the re-routing of the Kashgar and associated Pamir rivers towards the north into their present geometries. The uppermost Artux Formation, dated to ~11 Ma, is dominated by erosion from the North Kunlun which was actively uplifting at that time.

Collectively the data indicate a long and relatively old uplift history for the northwestern margin of the Tibetan Plateau. Most recently sediment appears to be transported directly from mountain sources into the Taklimakan Desert. Sediment dilution is significant because the rivers themselves recycle desert sediments soon after leaving their rocky headwater gorges, with the original bedrock source signals rapidly diluted as rivers flow farther into the Taklimakan Desert. There is little opportunity for sediment buffering in the headwater regions since we find limited terracing within the Kunlun valleys dating at ~2.6, 1.4 and 0.5 ka. These Late Holocene terraces are unlikely linked to anthropogenic activities but instead reflect changing moisture mostly supplied by extreme South Asian summer monsoon events.

ACKNOWLEDGEMENTS

PDC thanks the Charles T. McCord Chair in Petroleum Geology at Louisiana State University for support of this project. PB and KP thank Martina Schulz for processing the samples and acknowledge financial support from the Institute for Chemistry and Biology of the Marine Environment (ICBM) and the Max Planck Institute for Marine Microbiology

Figure Captions

Figure 1. Shaded topographic map of the western Tarim Basin showing the locations sampled for this study. Topographic data is SRTM plotted by GeoMapApp. Earthquake locations are shown from USGS catalogue, magnitude 5 and greater (larger dots indicate larger magnitude). Diagram shows major river channels and the outlines of the drainages. Yellow stars show OSL sampling locations. Green stars for samples with geochemical data and U-Pb zircon dates. Green stars with red outlines show samples that alos have apatite fission track data. Black lines show the river networks targeted in this study with the red lines showing the boundaries of these catchments in the mountains. White shaded regions show extent of major glaciers.

Figure 2. Tectonic map of the major blocks around the western Tarim Basin and Pamir. Modified after Robinson et al.(2004). Black lines show the river networks targeted in this study, with gray shading indicating the extent of the catchment in the headwaters.

Figure 3. Geological map of the western Tarim Basin, Kunlun and eastern Pamir showing the potential source regions of sediment into the basin. Terrane bounding faults from Figure 2 are shown in heavier line weight.

Figure 4. Field photographs showing the locations sampled for OSL dating. (A) and (B) mounds of windblown fine sand at Mazatag Ridge with trees stabilizing the top of the sediment (Samples 13062201 and 13062202). (C) fluvial terrace in the Kargilik River basin, which joins the Yarkand river in the Tarim basin (Sample 13062201), (D) Aerial photograph from Google Earth of the Kargilik River showing the locations of two terraces sampled upstream from that shown in C (Samples 13062202 and13062203). (E) fluvial terrace from the Kashgar River just to the west of Kashgar (Samples 13062701 and 13062703). (F) Aerial photograph of the Mazatag Ridge showing location of photographs A and B (black square) and the sand sea piled up on the north side.

Figure 5. A) Q-F-L ternary provenance discrimination diagrams of point counts. Diagrams indicate a dominantly recycled orogenic source terrane. Ternary diagram and fields modified from Dickinson et al. (1983). B) A-CN-K plot of Fedo et al. (1995) showing extremely low CIA values for all samples. Y = Yarkand (13062101), uH = Upper Hotan (13062401), lH = Lower Hotan (13062403), K = Kashgar (13062701), D = Dune sand (13062402). Kao = kaolinite, chl = chlorite, gb = gibbsite, sm = smectite, il = illite, m = muscovite, bi – biotite, ksp = K=feldspar, pl = plagioclase.

Figure 6. Sr isotope ratios plotted against ε_{Nd} values for our modern sediments. We also show the range of possible basement source rocks in the western Tarim Basin. Fields are define from source data is from Georoc, except for Songpan Garze turbidite sandstones which are from She et al. (2006), Karakoram data from Schärer et al. (1990), Kunlun Terrane data from Robinson et al. (2012) and Chang *et al*. (2000). Taklimakan sands are from Chang *et al*. (2000).

Figure 7. Radial plots showing the distribution of cooling ages from apatite fission track from samples considered in this study (Galbraith, 1990).

Figure 8. Kernel Density Estimate (KDE) plots of zircon U-Pb ages from the sample considered in this study showing the relative abundance of different aged crystals in each. Data from Kunlun basement and Cenozoic sediments is from Bershaw et al. (2012). Western Pamir Rivers are from Lukens et al. (2012). Tian Shan river data is from Rittner et al. (2016). Karakoram data is from the compilation of Clift et al. (2004), together with more recent data from Ravikant et al. (2009).

Figure 9. Annual mean rainfall and local topographic relief for the study area. (A) Annual rainfall values derived from TRMM 3B42 data from 1998–2009 at 0.25° × 0.25° resolution (http://www.geog.ucsb.edu/wbodo/TRMM/); (B) Mean local topographic relief calculated using a 20-km radius moving window from void-filled SRTM90 DEM. Blue lines denote stream network.

Figure 10. Stratigraphic diagram showing the proposed correlation between the Cenozoic stratigraphy of Zheng et al. (2015) and Cao et al. (2014).

Figure 11. Kernel Density Estimate (KDE) plots of zircon U-Pb ages spanning 600 Ma from the modern samples considered as part of this study compared with detrital zircons from older sedimentary rocks deposited along the northern edge of the Kunlun from Cao et al. (2014).

Figure 12. Multidimensional scaling (MDS) plot showing the Kolmogorov-Smirnov distances between sample zircon age spectra, following the method of Vermeesch (2013). New sediment samples are shown in green, with possible basement sources in yellow and Cenozoic sedimentary rocks in red.

777 Table 1. Sample numbers and locations.

778

779 Table 2. Bulk sediment major and trace element compositions, together with associated
780 Sr and Nd isotope ratios.

781

782 Table 3. Data and depositional ages from the OSL analysis of terrace sediments.

783

784

REFERENCES CITED

Aitchison, J. C., Ali, J. R., and Davis, A. S., 2007, When and where did India and Asia collide?: Journal of Geophysical Research, v. 112, no. B05423. doi:10.1029/2006JB004706.

Avouac, J. P., and Tapponnier, P., 1993, Kinematic Model of Active Deformation in Central-Asia: Geophysical Research Letters, v. 20, no. 10, p. 895-898.

Bershaw, J., Garzione, C. N., Schoenbohm, L., Gehrels, G., and Tao, L., 2012, Cenozoic evolution of the Pamir plateau based on stratigraphy, zircon provenance, and stable isotopes of foreland basin sediments at Oytag (Wuyitake) in the Tarim Basin (west China): Journal of Asian Earth Sciences, v. 44, p. 136–148. doi:10.1016/j.jseaes.2011.04.020.

Blöthe, J. H., and Korup, O., 2013, Millennial lag times in the Himalayan sediment routing system: Earth and Planetary Science Letters, v. 382, p. 38-46.

Bookhagen, B., Fleitmann, D., Nishiizumi, K., Strecker, M. R., and Thiede, R. C., 2006, Holocene monsoonal dynamics and fluvial terrace formation in the northwest Himalaya, India: Geology, v. 34, no. 7, p. 601-604.

Bosboom, R. E., Dupont-Nivet, G., Houben, A. J. P., Brinkhuis, H., Villa, G., Mandic, O., Stoica, M., Zachariasse, W.-J., Guo, Z., and Li, C., 2011, Late Eocene sea retreat from the Tarim Basin (west China) and concomitant Asian paleoenvironmental change: Palaeogeography, Palaeoclimatology, Palaeoecology, v. 299, p. 385–398.

Böthe, O., Fraedrich, K., and Zhu, X., 2012, Precipitation climate of Central Asia and the large-scale atmospheric circulation: Theoretical and Applied Climatology, v. 108, no. 3, p. 345-354.

Boulin, J., 1988, Hercynian and Eocimmerian events in Afghanistan and adjoining regions: Tectonophysics, v. 148, p. 253–278. doi:10.1016/0040- 1951(88)90134-5.

Burbank, D. W., Blythe, A. E., Putkonen, J., Pratt-Sitaula, B., Gabet, E., Oskins, M., Barros, A., and Ojha, T. P., 2003, Decoupling of erosion and precipitation in the Himalayas: Nature, v. 426, p. 652–655.

Burtman, V. S., and Molnar, P., 1993, Geological and Geophysical Evidence for Deep Subduction of Continental Crust Beneath the Pamir, Geological Society of America, Special Paper, 76 p.

Cao, K., Xu, Y., Wang, G., Zhang, K., van der Beek, P., Wang, C., Jiang, S., and Bershaw, J., 2014, Neogene Source-to-Sink Relations between the Pamir and Tarim Basin: Insights from Stratigraphy, Detrital Zircon Geochronology, and Whole-Rock Geochemistry: The Journal of Geology, v. 122, p. 433–454. doi: 10.1086/676478.

Chang, Q., Mishima, T., Yakubi, S., Takahashi, Y., and Shimizu, H., 2000, Sr and Nd isotope ratios and REE abundances of moraines in the mountain areas surrounding the Taklimakan Desert, NW China: Geochemical Journal, v. 34, no. 407-427.

Clift, P. D., Campbell, I. H., Pringle, M. S., Carter, A., Zhang, X., Hodges, K. V., Khan, A. A., and Allen, C. M., 2004, Thermochronology of the modern Indus River bedload; new insight into the control on the marine stratigraphic record: Tectonics, v. 23, no. TC5013. doi:10.1029/2003TC001559.

Clift, P. D., and Giosan, L., 2014, Sediment fluxes and buffering in the post-glacial Indus Basin: Basin Research, v. 25, p. 1–18. doi: 10.1111/bre.12038.

Clift, P. D., Hodges, K., Heslop, D., Hannigan, R., Hoang, L. V., and Calves, G., 2008, Greater Himalayan exhumation triggered by Early Miocene monsoon intensification: Nature Geoscience, v. 1, p. 875-880. doi:10.1038/ngeo351.

Dadson, S., Hovius, N., Chen, H., Dade, W. B., Hsieh, M. L., Willett, S., Hu, J. C., Horng, M. J., Chen, M. C., Stark, C. P., Lague, D., and Lin, J. C., 2003, Links between erosion, runoff variability and seismicity in the Taiwan orogen: Nature, no. 426, p. 648–651.

DePaolo, D. J., and Wasserburg, G. J., 1976, Nd isotopic variations and petrogenetic models: Geophysical Research Letters, v. 3, no. 5, p. 249-252.

Derry, L. A., and France-Lanord, C., 1996, Neogene Himalayan weathering history and river $^{87}Sr/^{86}Sr$; impact on the marine Sr record: Earth and Planetary Science Letters, v. 142, p. 59-74.

Dickinson, W. R., Beard, S. L., Brackenridge, G. R., Erjavec, J. L., Ferguson, R. C., Inman, K. F., Knepp, R. A., Lindberg, F. A., and Ryber, P. T., 1983, Provenance of North American Phanerozoic sandstones in relation to tectonic setting: Geological Society of America Bulletin, v. 94, p. 222-235.

Dixit, Y., Hodell, D. A., and Petrie, C. A., 2014, Abrupt weakening of the summer monsoon in northwest India <4100 yr ago: Geology. DOI:10.1130/G35236.1.

Dortch, J. M., Dietsch, C., Owen, L. A., Caffee, M. W., and Ruppert, K., 2011, Episodic fluvial incision of rivers and rock uplift in the Himalaya and Transhimalaya: Journal of the Geological Society, v. 168, p. 783-804.

Duvall, A. R., Clark, M. K., Avdeev, B., Farley, K. A., and Chen, Z., 2012, Widespread late Cenozoic increase in erosion rates across the interior of eastern Tibet constrained by detrital low-temperature thermochronometry: Tectonics, v. 31, no. TC3014. doi:10.1029/2011TC002969.

Fedo, C. M., Nesbitt, H. W., and Young, G. M., 1995, Unraveling the effects of potassium metasomatism in sedimentary rocks and paleosols, with implications for paleoweathering conditions and provenance: Geology, v. 23, p. 921–924.

Feng, Z.-D., An, C. B., and Wang, H. B., 2006, Holocene climatic and environmental changes in the arid and semi-arid areas of China: a review: The Holocene, v. 16, no. 1, p. 119-130. doi: 10.1191/0959683606hl912xx.

Foster, D. A., Gleadow, A. J. W., and Mortimer, G., 1994, Rapid Pliocene exhumation in the Karakoram (Pakistan), revealed by fission-track thermochronology of the K2 gneiss: Geology, v. 22, no. 1, p. 19-22.

Fuchs, M., and Owen, L. A., 2008, Luminescence dating of glacial and associated sediments: review, recommendations and future directions: Boreas, v. 37, p. 636-659.

Galbraith, R. F., 1990, The radial plot: Graphical assessment of spread in ages Nuclear Tracks and Radiation Measurement, v. 17, p. 207–214.

Garçon, M., Chauvel, C., France-Lanord, C., Huyghe, P., and Lavé, J., 2013, Continental sedimentary processes decouple Nd and Hf isotopes: Geochimica et Cosmochimica Acta, v. 121, p. 177-195.

Garçon, M., Chauvel, C., France-Lanord, C., Limonta, M., and Garzanti, E., 2014, Which minerals control the Nd–Hf–Sr–Pb isotopic compositions of river sediments?: Chemical Geology, v. 364, p. 42–55. doi:10.1016/j.chemgeo.2013.11.018.

875 Garzanti, E., Andó, S., France-Lanord, C., Censi, P., Vignola, P., Galy, V., and Lupker,
876 M., 2011, Mineralogical and chemical variability of fluvial sediments 2.
877 Suspended-load silt (Ganga–Brahmaputra, Bangladesh): Earth and Planetary
878 Science Letters, v. 302, p. 107–120. doi:10.1016/j.epsl.2010.11.043.
879 Gehrels, G. E., 2014, Detrital Zircon U-Pb Geochronology Applied to Tectonics: Annual
880 Review of Earth and Planetary Sciences, v. 42, p. 127-149. doi: 10.1146/annurev-
881 earth-050212-124012.
882 Goldstein, S. L., O'Nions, R. K., and Hamilton, P. J., 1984, A Sm-Nd isotopic study of
883 atmospheric dusts and particulates from major river systems: Earth and Planetary
884 Science Letters, v. 70, no. 2, p. 221-236.
885 Green, P. F., 1989, Thermal and tectonic history of the East Midlands shelf (onshore UK)
886 and surrounding regions assessed by apatite fission track analysis: Journal of the
887 Geological Society, v. 146, p. 755-773.
888 Hartmann, K., and Wünnemann, B., 2009, Hydrological changes and Holocene climate
889 variations in NW China, inferred from lake sediments of Juyanze palaeolake by
890 factor analyses: Quaternary International, v. 194, no. 1–2, p. 28–44.
891 doi:10.1016/j.quaint.2007.06.037.
892 Holmes, J. A., Cook, E. R., and Yang, B., 2009, Climate change over the past 2000 years
893 in Western China: Quaternary International, v. 194, no. 1–2, p. 91–107.
894 doi:10.1016/j.quaint.2007.10.013.
895 Hubbard, M. S., Grew, E. S., Hodges, K. V., Yates, M. G., and Pertsev, N. N., 1999,
896 Neogene cooling and exhumation of upper-amphibolite-facies 'whiteschists' in
897 the southwest Pamir Mountains, Tajikistan: Tectonophysics, v. 305, p. 325–337.
898 doi:10.1016/S0040-1951(99)00012-8.
899 Ingersoll, R. V., Bullard, T. F., Ford, R. L., Grimm, J. P., Pickle, J. D., and Sares, S. W.,
900 1984, The effect of grain size on detrital modes: A test of the Gazzi-Dickinson
901 point-counting method: Journal of Sedimentary Petrology, v. 54, p. 103-116.
902 Jacobsen, S. B., and Wasserburg, G. J., 1980, Sm-Nd isotopic evolution of chondrites:
903 Earth and Planetary Science Letters v. 50, no. 1, p. 139-155.
904 Jolivet, M., Brunel, M., Seward, D., Xu, Z., Yang, J., Roger, F., Tapponnier, P.,
905 Malavieille, J., Arnaud, N., and Wu, C., 2001, Mesozoic and Cenozoic tectonics
906 of the northern edge of the Tibetan plateau: fission-track constraints:
907 Tectonophysics, v. 343, no. 1–2, p. 111–134. doi:10.1016/S0040-1951(01)00196-
908 2.
909 Jonell, T. N., Clift, P. D., Hoang, L. V., Hoang, T., Carter, A., Wittmann, H., Böning, P.,
910 Pahnke, K., and Rittenour, T., 2016, Controls on Erosion Patterns and Sediment
911 Transport in a Monsoonal, Tectonically Quiescent Drainage, Song Gianh, Central
912 Vietnam: Basin Research. doi: 10.1111/bre.12199.
913 Kapp, P., DeCelles, P. G., Gehrels, G. E., Heizler, M., and Ding, L., 2007, Geological
914 records of the Lhasa-Qiangtang and Indo-Asian collisions in the Nima area of
915 central Tibet: Geological Society of America Bulletin, v. 119, p. 917–933.
916 doi:10.1130/B26033.1.
917 Kapp, P., Yin, A., Harrison, T. M., and Ding, L., 2005, Cretaceous-Tertiary shortening,
918 basin development, and volcanism in central Tibet: Geological Society of
919 America Bulletin, v. 117, no. 7-8, p. 865-878.

Karim, A., and Veizer, J., 2002, Water balance of the Indus river basin and moisture source in the Karakoram and western Himalayas: implications from hydrogen and oxygen isotopes river water: Journal of Geophysical Research, v. 107, no. D18. doi:10.1029/2000JD000253.

Kirstein, L. A., Sinclair, H. D., Stuart, F. M., and Dobson, K., 2006, Rapid early Miocene exhumation of the Ladakh batholith, western Himalaya: Geology, v. 34, no. 12, p. 1049–1052. doi: 10.1130/G22857A.

Kutzbach, J. E., Prell, W. L., and Ruddiman, W. F., 1993, Sensitivity of Eurasian climate to surface uplift of the Tibetan Plateau: Journal of Geology, v. 101, p. 177–190.

Lukens, C. E., Carrapa, B., Singer, B. S., and Gehrels, G., 2012, Miocene exhumation of the Pamir revealed by detrital geothermochronology of Tajik rivers: Tectonics, v. 31, no. TC2014. doi:10.1029/2011TC003040.

McDougall, I., and Harrison, T. M., 1999, Geochronology and Thermochronology by the 40Ar/39Ar Method, Oxford, UK, Oxford University Press.

Molnar, P., England, P., and Martinod, J., 1993, Mantle Dynamics, Uplift of the Tibetan Plateau, and the Indian Monsoon: Reviews of Geophysics, v. 31, no. 4, p. 357-396.

Munack, H., Korup, O., Resentini, A., Limonta, M., Garzanti, E., Blöthe, J. H., Scherler, D., Wittmann, H., and Kubik, P. W., 2014, Postglacial denudation of western Tibetan Plateau margin outpaced by long-term exhumation: Geological Society of America Bulletin, v. 126, p. 1580-1594. doi: 10.1130/B30979.1.

Murphy, M. A., Yin, A., Kapp, P., Harrison, T. M., Ding, L., and Guo, J., 2000, Southward propagation of the Karakoram fault system, Southwest Tibet; timing and magnitude of slip: Geology (Boulder), v. 28, no. 5, p. 451-454.

Murray, A. S., and Wintle, A. G., 2000, Luminescence dating of quartz using an improved single-aliquot regenerative-dose protocol: Radiation Measurements, v. 32, p. 57-72.

Najman, Y., Appel, E., Boudagher‐Fadel, M., Bown, P., Carter, A., Garzanti, E., Godin, L., Han, J., Liebke, U., Oliver, G., Parrish, R., and Vezzoli, G., 2010, Timing of India‐Asia collision: Geological, biostratigraphic, and palaeomagnetic constraints: Journal of Geophysical Research. doi:10.1029/2010JB007673.

Nesbitt, H. W., Markovics, G., and Price, R. C., 1980, Chemical processes affecting alkalis and alkaline earths during continental weathering: Geochimica et Cosmochimica Acta, v. 44, p. 1659–1666.

Peltzer, G., and Tapponnier, P., 1988, Formation and evolution of strike-slip faults, rifts, and basins during the India-Asia Collision: an experimental approach: Journal of Geophysical Research, v. 93, p. 15085-15117.

Phillips, R. J., Parrish, R. R., and Searle, M. P., 2004, Age constraints on ductile deformation and long-term slip rates along the Karakoram fault zone, Ladakh: Earth and Planetary Science Letters, v. 226, p. 305-319.

Ravikant, V., Wu, F. Y., and Ji, W. Q., 2009, Zircon U-Pb and Hf isotopic constraints on petrogenesis of the Cretaceous-Tertiary granites in eastern Karakoram and Ladakh, India: Lithos, v. 110, p. 153-166.

Reiners, P. W., Ehlers, T. A., Mitchell, S. G., and Montgomery, D. R., 2003, Coupled spatial variations in precipitation and long-term erosion rates across the Washington Cascades: Nature, v. 426, no. 6967, p. 645-647.

965 Rhodes, E. J., 2011, Optically Stimulated Luminescence Dating of Sediments over the
966 Past 200,000 Years: Annual Review of Earth and Planetary Sciences, v. 39, p.
967 461-488. doi: 10.1146/annurev-earth-040610-133425.
968 Rittenour, T. M., 2008, Luminescence dating of fluvial deposits: applications to
969 geomorphic, palaeoseismic and archaeological research: Boreas v. 37, p. 613-635.
970 Rittner, M., Vermeesch, P., Carter, A., Bird, A., Stevens, T., Garzanti, E., Andò, S.,
971 Vezzoli, G., Dutt, R., Xu, Z., and Lu, H., 2016, The provenance of Taklamakan
972 desert sand: Earth and Planetary Science Letters, v. 437, no. 1, p. 127–137.
973 doi:10.1016/j.epsl.2015.12.036.
974 Robinson, A. C., Ducea, M., and Lapen, T. J., 2012, Detrital zircon and isotopic
975 constraints on the crustal architecture and tectonic evolution of the northeastern
976 Pamir: Tectonics, v. 31, no. TC2016. doi:10.1029/2011TC003013.
977 Robinson, A. C., Yin, A., Manning, C. E., Harrison, T. M., Zhang, S.-H., and Wang, X.-
978 F., 2004, Tectonic evolution of the northeastern Pamir: Constraints from the
979 northern portion of the Cenozoic Kongur Shan extensional system, western China:
980 Geological Society of America Bulletin, v. 116, no. 7-8, p. 953-973. doi:
981 10.1130/B25375.1.
982 Robinson, A. C., Yin, A., Manning, C. E., Harrison, T. M., Zhang, S.-H., and Wang, X.-
983 F., 2007, Cenozoic evolution of the eastern Pamir: Impli- cations for the strain-
984 accommodation mechanisms at the western end of the Himalayan-Tibetan orogen:
985 Geological Society of America Bulletin, v. 119, p. 882–896.
986 doi:10.1130/B25981.1.
987 Schärer, U., Copeland, P., Harrison, T. M., and Searle, M. P., 1990, Age, cooling history,
988 and origin of post-collisional leucogranites in the Karakoram Batholith; a multi-
989 system isotope study: Journal of Geology, v. 98, no. 2, p. 233–251.
990 Schulz, H.-M., Bechtel, A., and Sachsenhofer, R. F., 2005, The birth of the Paratethys
991 during the Early Oligocene: from Tethys to an ancient Black Sea analogue?:
992 Global and Planetary Change, v. 49, p. 163–176.
993 Searle, M. P., 1991, Geology and Tectonics of the Karakoram Mountains, Chichester,
994 John Wiley and Sons.
995 Searle, M. P., Parrish, R. R., Tirrul, R., and Rex, D. C., 1990, Age of crystallization of the
996 K2 gneiss in the Baltoro Karakoram: Journal of the Geological Society, v. 147, p.
997 603–606.
998 Searle, M. P., and Phillips, R. J., 2007, Relationships between right-lateral shear along
999 the Karakoram Fault and metamorphism, magmatism, exhumation and uplift;
1000 evidence from the K2-Gasherbrum-Pangong ranges, north Pakistan and Ladakh:
1001 Journal of the Geological Society, v. 164, no. 2, p. 439-450.
1002 Searle, M. P., Rex, A. J., Tirrul, R., Rex, D. C., Barnicoat, A., and Windley, B. F., 1989,
1003 Metamorphic, magmatic and tectonic evolution of the Central Karakoram in the
1004 Biafo-Baltoro-Hushe regions of north Pakistan: Geological Society of America
1005 Special Paper, v. 232, p. 47-73.
1006 Sengor, A. M. C., and Natal'in, B. A., 1996, Paleotectonics of Asia: fragments of a
1007 synthesis, *in* Yin, A., and Harrison, M., eds., The Tectonic Evolution of Asia:
1008 Cambridge, Cambridge University Press,, p. 486-640.
1009 Shao, Y., Wyrwoll, K.-H., Chappell, A., Huang, J., Lin, Z., McTainsh, G. H., Mikami, M.,
1010 Tanaka, T. Y., Wang, X., and Yoon, S., 2011, Dust cycle: An emerging core

1011 theme in Earth system science: Aeolian Research, v. 2, no. 4, p. 181–204.
1012 doi:10.1016/j.aeolia.2011.02.001.
1013 She, Z., Ma, C., Mason, R., Li, J., Wang, G., and Lei, Y., 2006, Provenance of the
1014 Triassic Songpan–Ganzi flysch, west China: Chemical Geology, v. 231, no. 1–2, p.
1015 159–175. doi:10.1016/j.chemgeo.2006.01.001.
1016 Sobel, E. R., Chen, J., and Heermance, R. V., 2006a, Late Oligocene–Early Miocene
1017 initiation of shortening in the Southwestern Chinese Tian Shan: Implications for
1018 Neogene shortening rate variations: Earth and Planetary Science Letters, v. 247,
1019 no. 1-2, p. 70-81.
1020 Sobel, E. R., and Dumitru, T. A., 1997, Thrusting and exhumation around the margins of
1021 the western Tarim basin during the India-Asia collision: Journal of Geophysical
1022 Research, v. 102, no. B3, p. 5043–5063. doi:10.1029/96JB03267.
1023 Sobel, E. R., Oskin, M., Burbank, D., and Mikolaichuk, A., 2006b, Exhumation of
1024 basement-cored uplifts: Example of the Kyrgyz Range quantified with apatite
1025 fission track thermochronology: Tectonics, v. 25, no. TC2008.
1026 doi:10.1029/2005TC001809.
1027 Sun, J., Xiao, W., Windley, B. F., Ji, W., Fu, B., Wang, J., and Jin, C., 2016, Provenance
1028 change of sediment input in the northeastern foreland of Pamir related to collision
1029 of the Indian plate with the Kohistan-Ladakh arc at around 47 Ma: Tectonics. doi:
1030 10.1002/2015TC003974.
1031 Tada, R., Zheng, H., and Clift, P. D., 2016, Evolution and variability of the Asian
1032 monsoon and its potential linkage with uplift of the Himalaya and Tibetan
1033 Plateau: Progress in Earth and Planetary Science, v. 3, no. 4, p. 1-26. doi
1034 10.1186/s40645-016-0080-y.
1035 Tada, R., Zheng, H., Sugiura, N., Isozaki, Y., Hasegawa, H., Sun, Y., Yang, W., Wang,
1036 K., and Toyoda, S., 2010, Desertification and dust emission history of the Tarim
1037 Basin and its relation to the uplift of northern Tibet, Volume 342: London,
1038 Geological Society,, Special Publications, p. 45-65.
1039 Tang, W., Zhang, Z., Li, J., Li, K., Luo, Z., and Chen, Y., 2015, Mesozoic and Cenozoic
1040 uplift and exhumation of the Bogda Mountain, NW China: Evidence from apatite
1041 fission track analysis: Geoscience Frontiers, v. 6, no. 4, p. 617–625.
1042 doi:10.1016/j.gsf.2014.04.006.
1043 Tapponnier, P., 2002, Oblique stepwise growth of the Tibet Plateau: Science, v. 295, no.
1044 5553, p. 277-277.
1045 Tapponnier, P., Mattauer, M., Proust, F., and Cassaigneau, C., 1981, Mesozoic ophiolites,
1046 sutures, and large-sale tectonic movements in Afghanistan: Earth and Planetary
1047 Science Letters, v. 52, p. 355–371. doi:10.1016/0012- 821X(81)90189-8.
1048 Uno, I., Eguchi, K., Yumimoto, K., Takemura, T., Shimizu, A., Uematsu, M., Liu, Z.,
1049 Wang, Z., Hara, Y., and Sugimoto, N., 2009, Asian dust transported one full
1050 circuit around the globe: Nature Geoscience, v. 2, p. 557-560
1051 doi:10.1038/ngeo583.
1052 Vermeesch, P., 2004, How many grains are needed for a provenance study?: Earth and
1053 Planetary Science Letters, v. 224, p. 351–441.
1054 Vermeesch, P., 2013, Multi-sample comparison of detrital age distributions: Chemical
1055 Geology, v. 341, p. 140–146. doi:10.1016/j.chemgeo.2013.01.010.

Wallis, D., Carter, A., Phillips, R. J., Parsons, A. J., and Searle, M. P., 2016, Spatial variation in exhumation rates across Ladakh and the Karakoram: New apatite fission track data from the Eastern Karakoram, NW India: Tectonics, v. 35, p. 704–721. doi:10.1002/2015TC003943.

Wang, E., Kirby, E., Furlong, K. P., Soest, M. v., Xu, G., Shi, X., Kamp, P. J. J., and Hodges, K. V., 2012, Two-phase growth of high topography in eastern Tibet during the Cenozoic: Nature Geoscience, v. 5, p. 640–645. doi:10.1038/ngeo1538.

Wang, E., Wan, J., and Liu, J., 2003, Late Cenozoic geological evolution of the foreland basin bordering the West Kunlun range in Pulu area: Constraints on timing of uplift of northern margin of the Tibetan Plateau: Journal of Geophysical Research, v. 108, no. B8, p. 2156-2202. doi:10.1029/2002JB001877.

Whipple, K. X., 2009, The influence of climate on the tectonic evolution of mountain belts Nature Geoscience, v. 2, p. 1-8. doi: 10.1038/ngeo413.

Wobus, C. W., Hodges, K. V., and Whipple, K. X., 2003, Has focused denudation sustained active thrusting at the Himalayan topographic front?: Geology, v. 31, no. 10, p. 861-864.

Wünnemann, B., Demske, D., Tarasov, P., Kotlia, B. S., Reinhardt, C., Bloemendal, J., Diekmann, B., Hartmann, K., Krois, J., Riedel, F., and Arya, N., 2010, Hydrological evolution during the last 15 kyr in the Tso Kar lake basin (Ladakh, India), derived from geomorphological, sedimentological and palynological records: Quaternary Science Reviews, v. 29, p. 1138-1155.

Wünnemann, B., Mischke, S., and Chen, F., 2006, A Holocene sedimentary record from Bosten Lake, China Palaeogeography, Palaeoclimatology, Palaeoecology, v. 234, p. 223–238. doi:10.1016/j.palaeo.2005.10.016.

Wyshnytzky, C. E., Rittenour, T. M., Nelson, M. S., and Thackray, G., 2015, Luminescence dating of late Pleistocene proximal glacial sediments in the Olympic Mountains, Washington: Quaternary International, v. 362, p. 116–123. doi:10.1016/j.quaint.2014.08.024.

Yang, S., Zhang, F., and Wang, Z., 2012, Grain size distribution and age population of detrital zircons from the Changjiang (Yangtze) River system, China: Chemical Geology, v. 296-297, p. 26-38.

Yang, X., Zhu, B., and White, P. D., 2007, Provenance of aeolian sediment in the Taklamakan Desert of western China, inferred from REE and major-elemental data: Quaternary International, v. 175, p. 71–85. doi:10.1016/j.quaint.2007.03.005.

Yatagai, A., and Yasunari, T., 1998, Variation of Summer Water Vapor Transport Related to Precipitation over and around the Arid Region in the Interior of the Eurasian Continent: Journal of the Meteorological Society of Japan, v. 76, no. 5, p. 799-815.

Yin, A., and Harrison, T. M., 2000, Geologic evolution of the Himalayan-Tibetan orogen: Annual Review of Earth and Planetary Sciences, v. 28, p. 211-280.

Zhang, R., Jiang, D., Zhang, Z., and Yu, E., 2015, The impact of regional uplift of the Tibetan Plateau on the Asian monsoon climate: Palaeogeography, Palaeoclimatology, Palaeoecology, v. 417, p. 137–150. doi:10.1016/j.palaeo.2014.10.030.

Zheng, H., Powell, C. M., An, Z., Zhou, J., and Dong, G.-r., 2000, Pliocene uplift of the northern Tibetan Plateau: Geology, v. 28, no. 8, p. 715-718.

Zheng, H., Tada, R., Jia, J., Lawrence, C., and Wang, K., 2010, Cenozoic sediments in the southern Tarim Basin: implications for the uplift of northern Tibet and evolution of the Taklimakan Desert, *in* Clift, P. D., Tada, R., and Zheng, H., eds., Monsoon evolution and tectonic-climate linkage in Asia, Volume 342, Geological Society.

Zheng, H., Wei, X., Tada, R., Clift, P. D., Wang, B., Jourdan, F., Wang, P., and He, M., 2015, Late Oligocene–early Miocene birth of the Taklimakan Desert: Proceedings of the National Academy of Sciences. doi:10.1073/pnas.1424487112.

Figure 1

Click here to download Figure Fig_1_Xinjiang Rivers Base Map (3).pdf

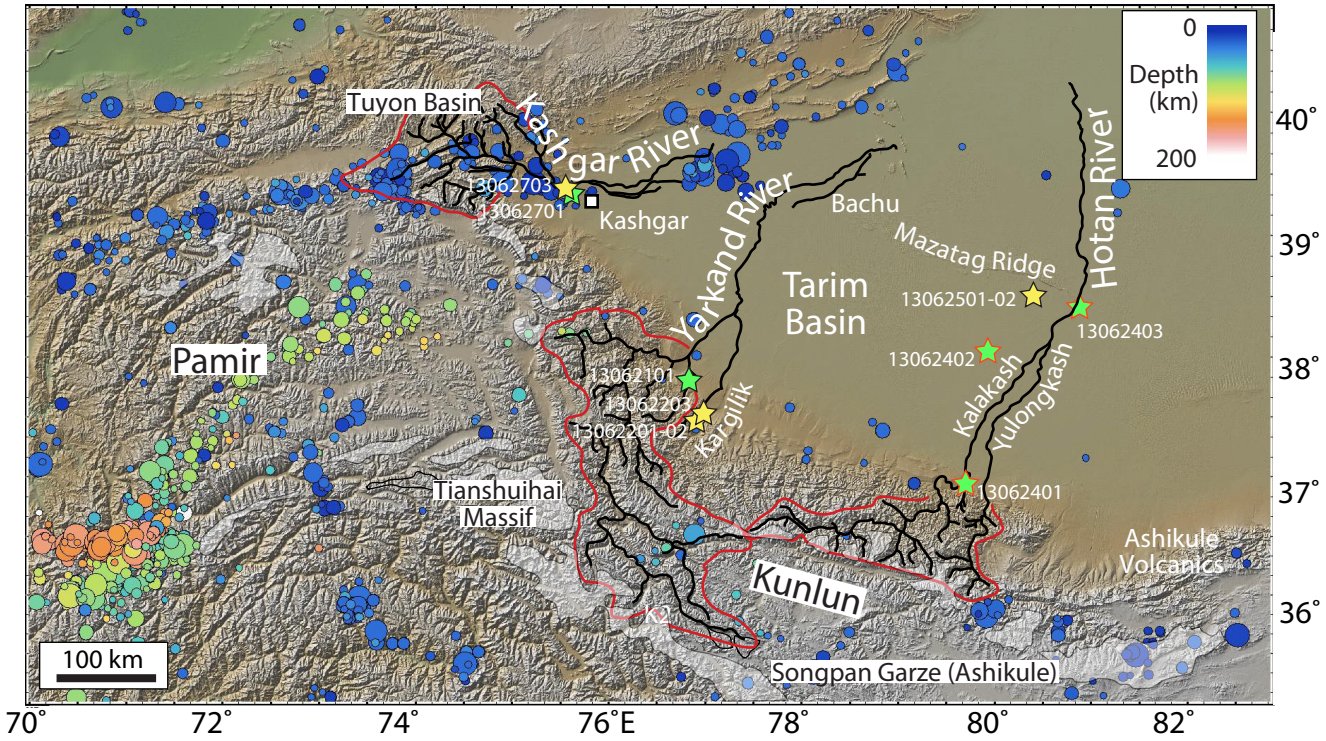

Figure 1
Clift et al.

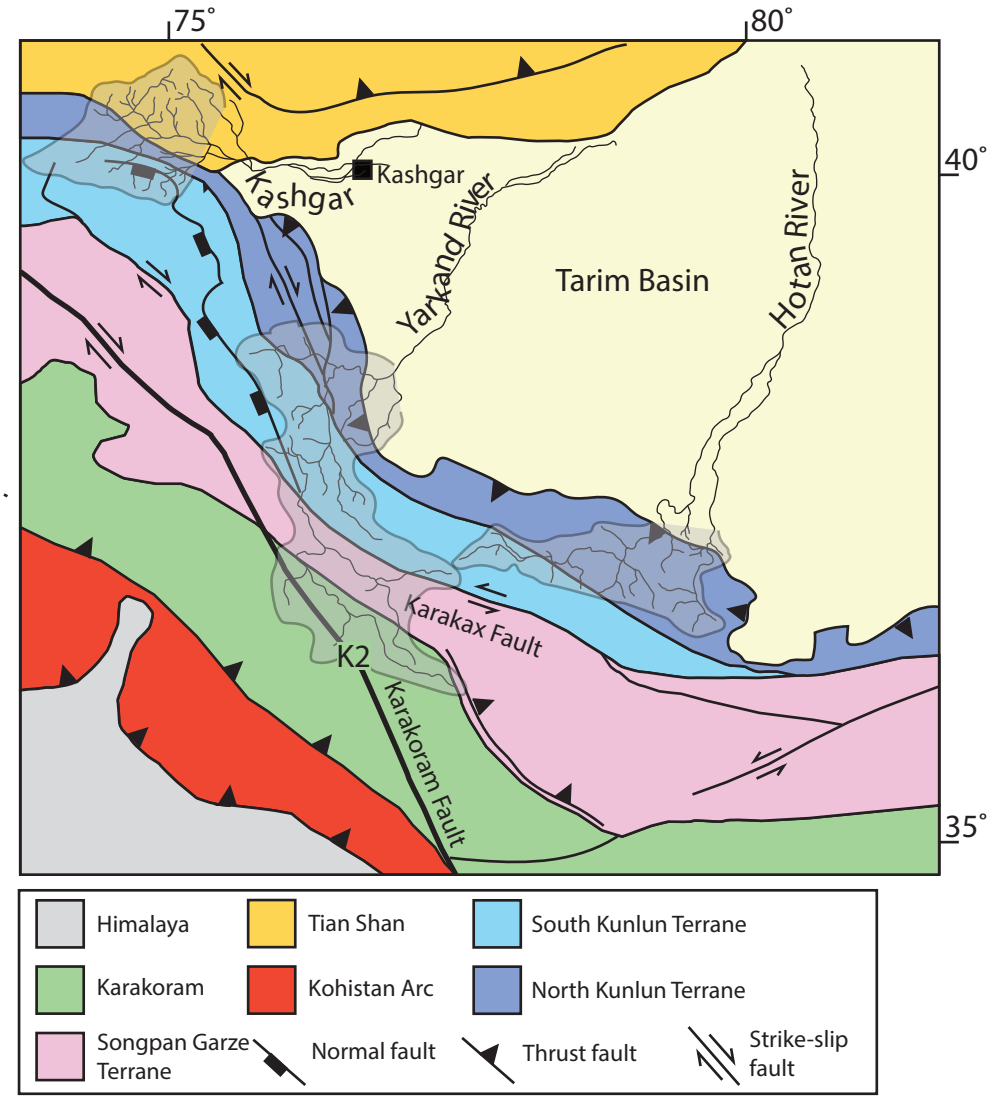

Figure 2
Clift et al.

Figure 3

Click here to download Figure Fig_3_Tarim Geology.jpg

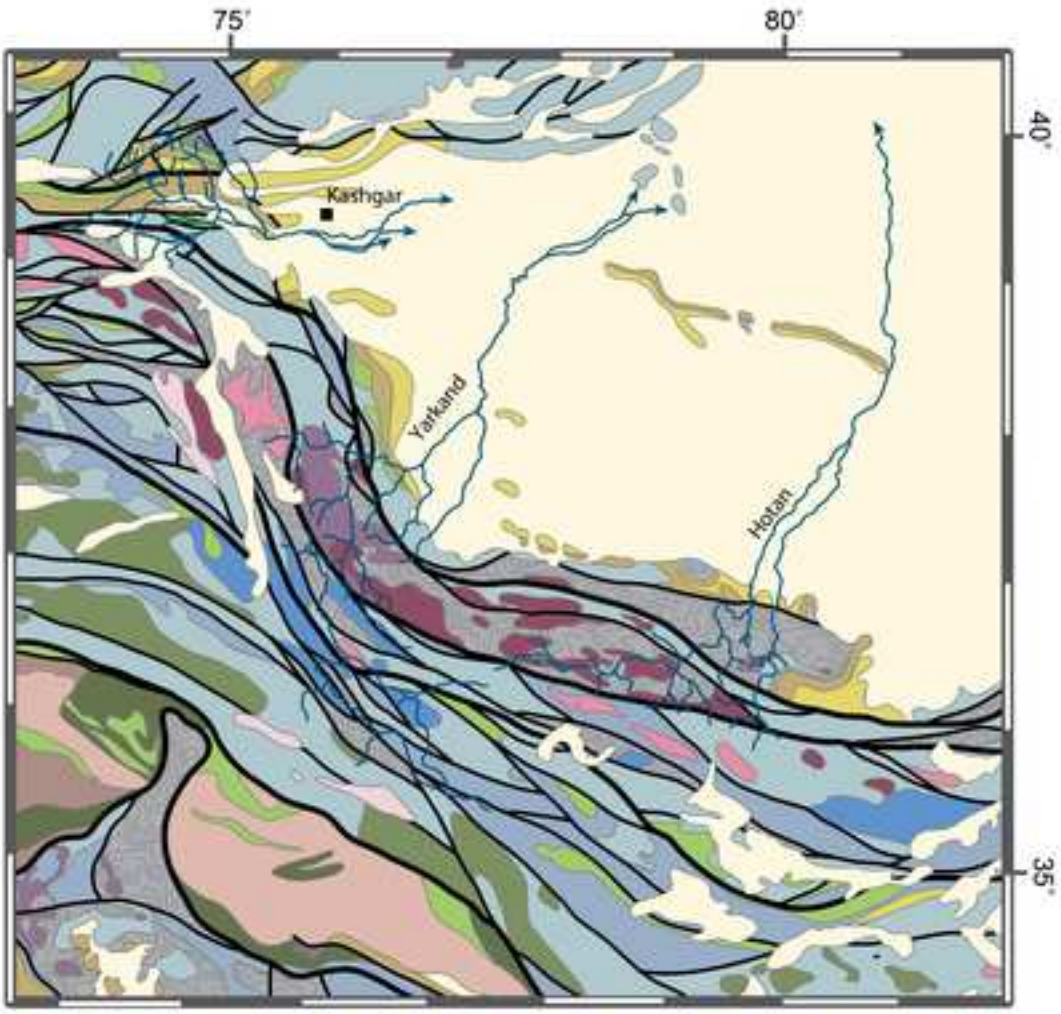

Sedimentary

- Quaternary sediments
- Neogene sedimentary
- Paleogene sedimentary
- Cretaceous sedimentary
- Triassic-Jurassic sedimentary
- Paleozoic sedimentary

terrain bounding fault

fault

river

Crystalline

- Neogene intrusions
- Paleogene intrusions
- Late K- E. Paleogene intrusions (felsic)
- Late K-E. Paleogene intrusions (mafic)
- Cretaceous volcanics
- Early Cretaceous intrusions
- Jurassic intrusions
- Late Paleozoic intrusions
- Early Paleozoic intrusions
- Proterozoic metamorphic

Figure 3
Clift et al.

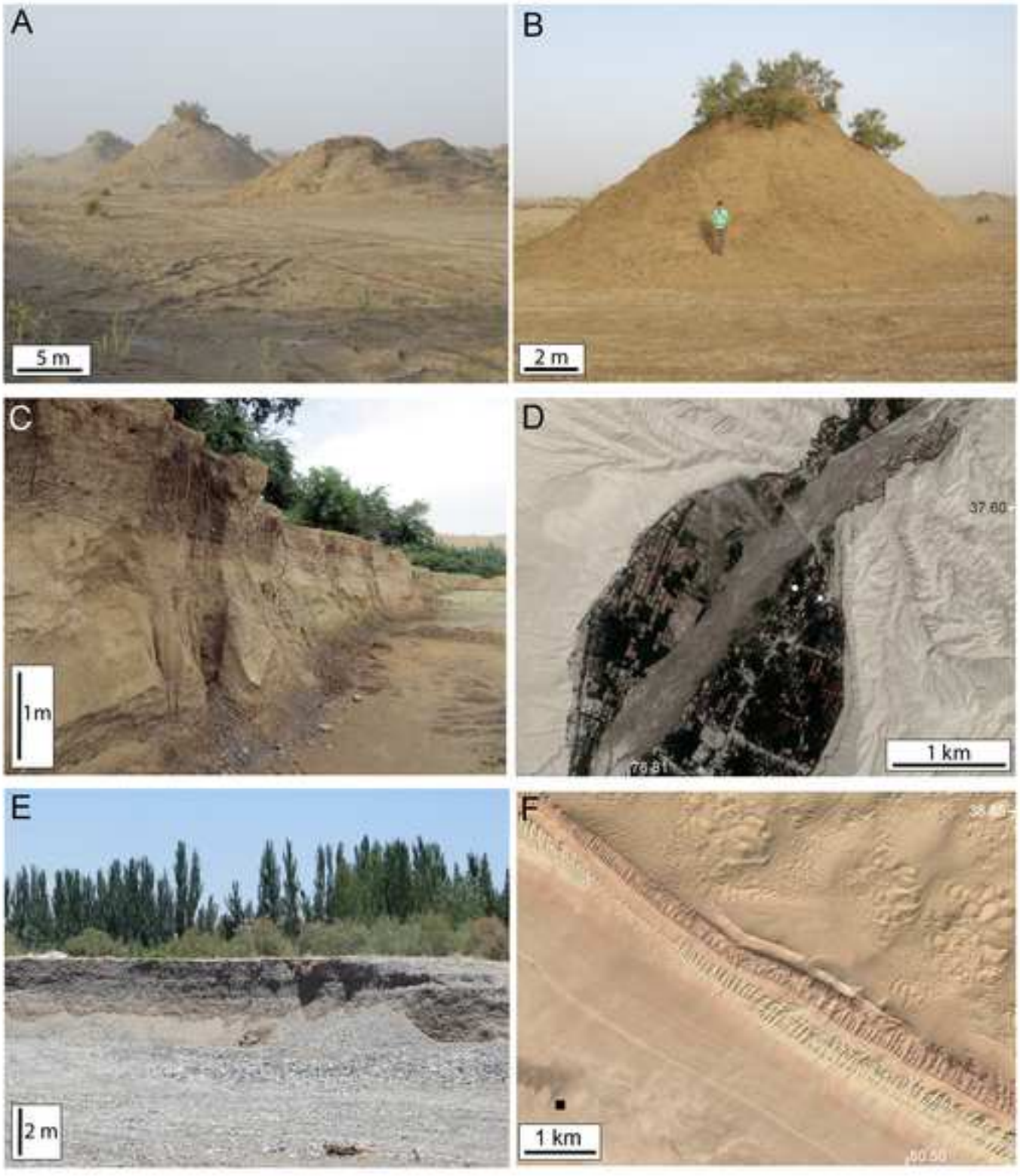

Figure 4
Clift et al.

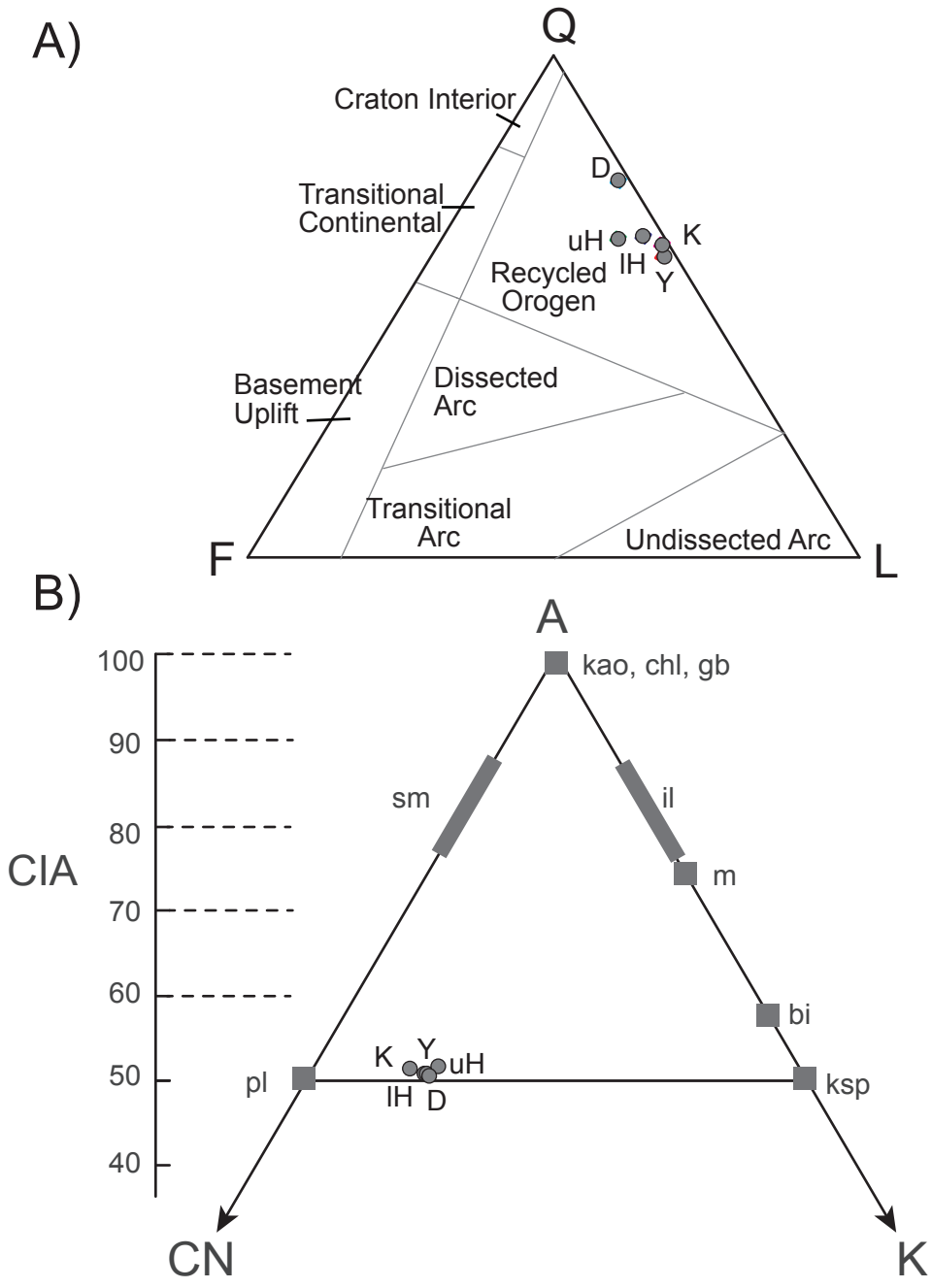

Figure 5
Clift et al.

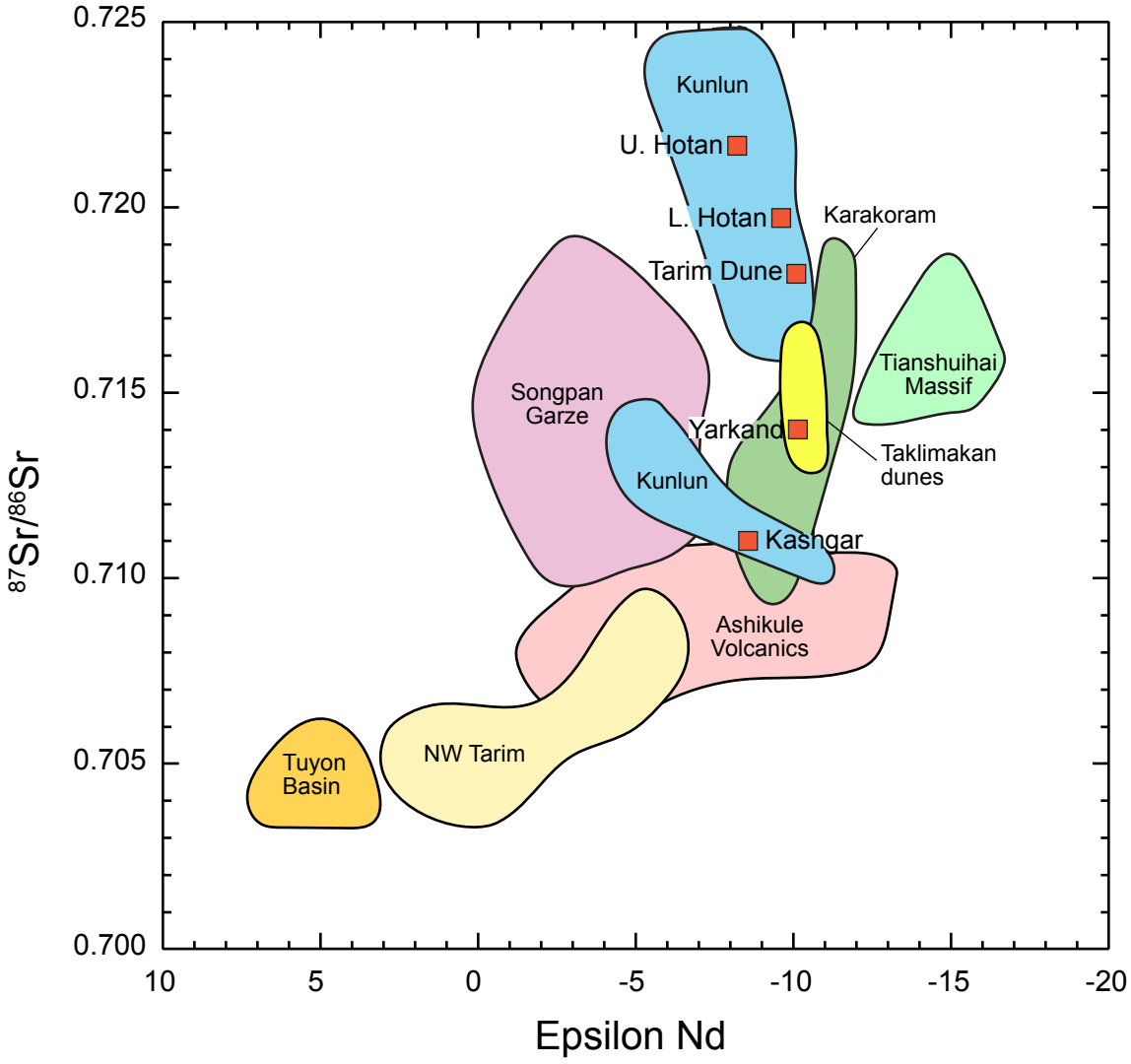

Figure 6
Clift et al.

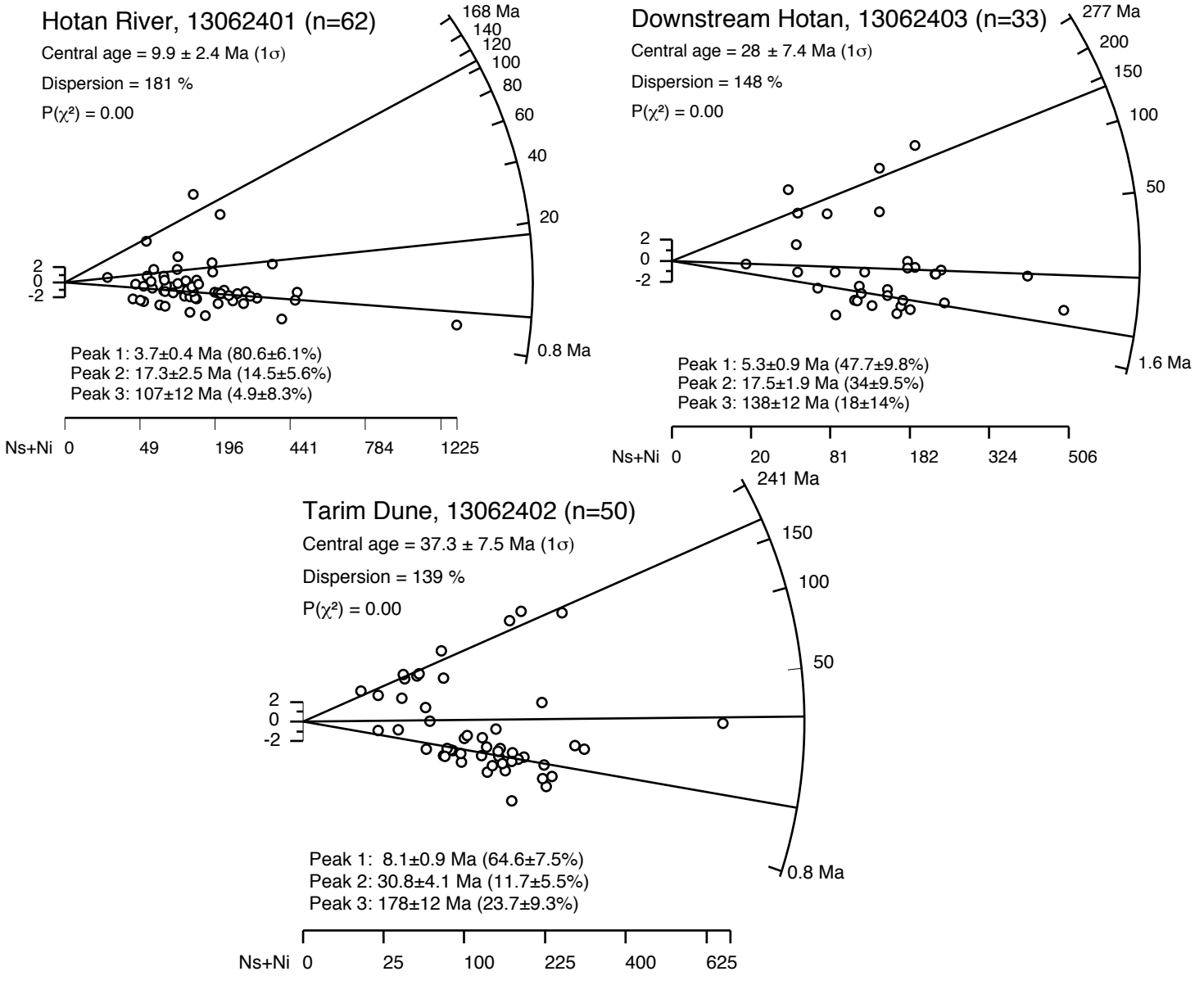

Figure 7
Clift et al.

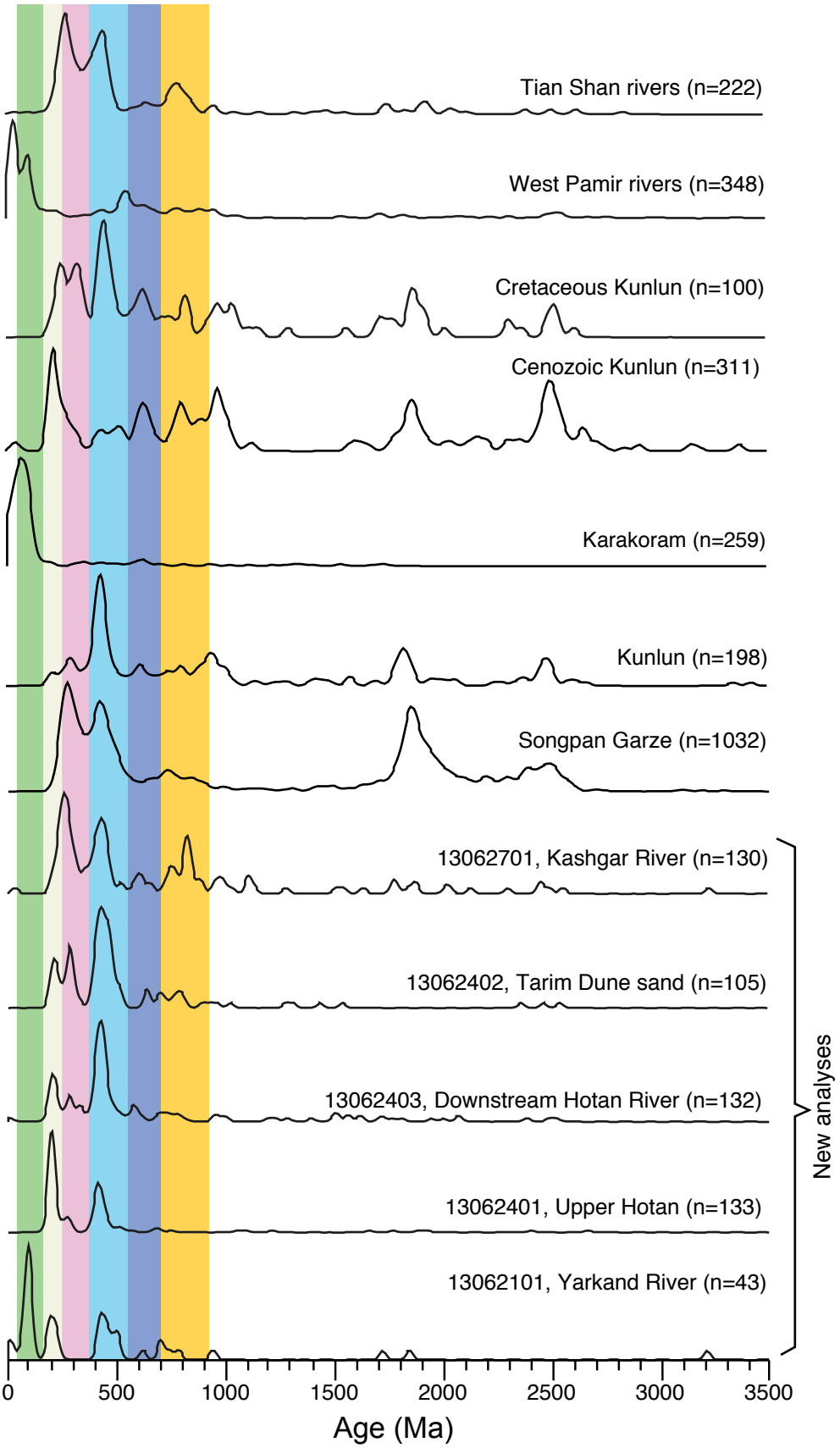

Figure 9
Clift et al.

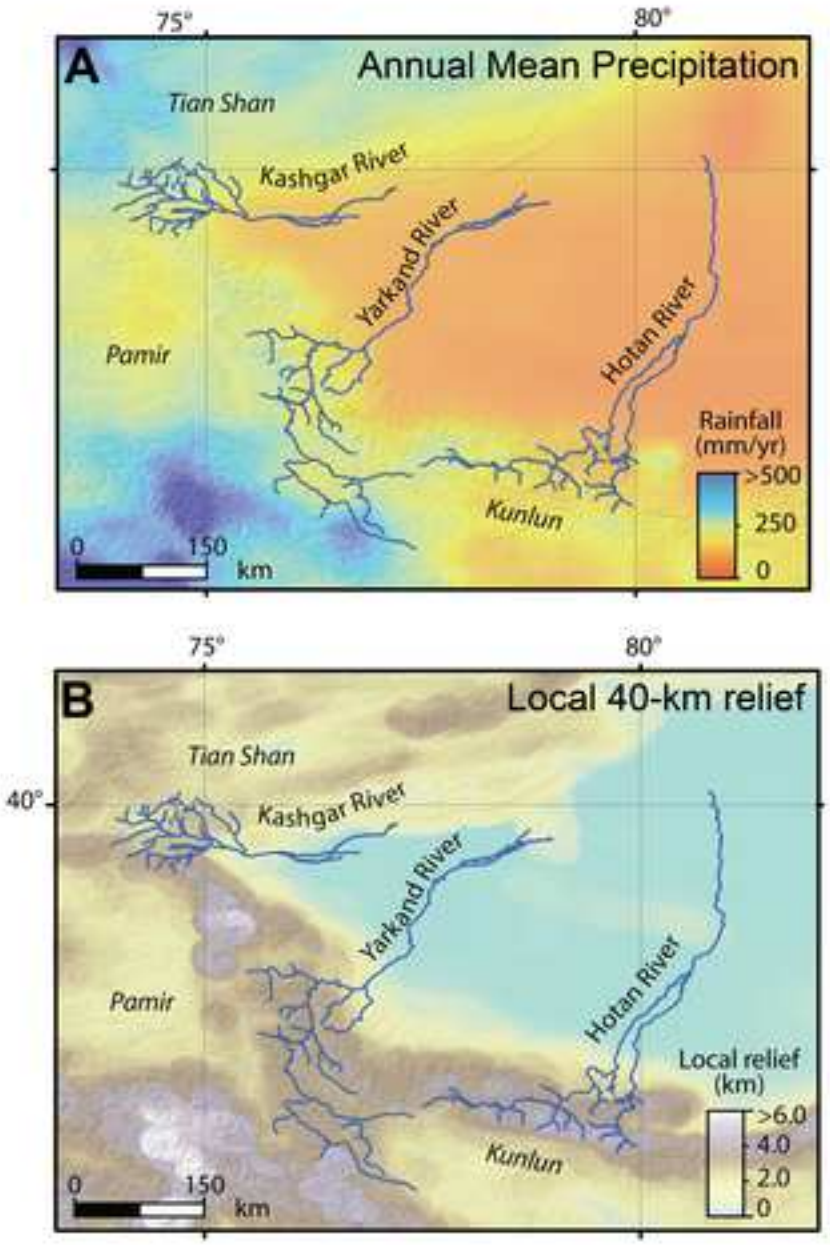

Figure 9
Clift et al.

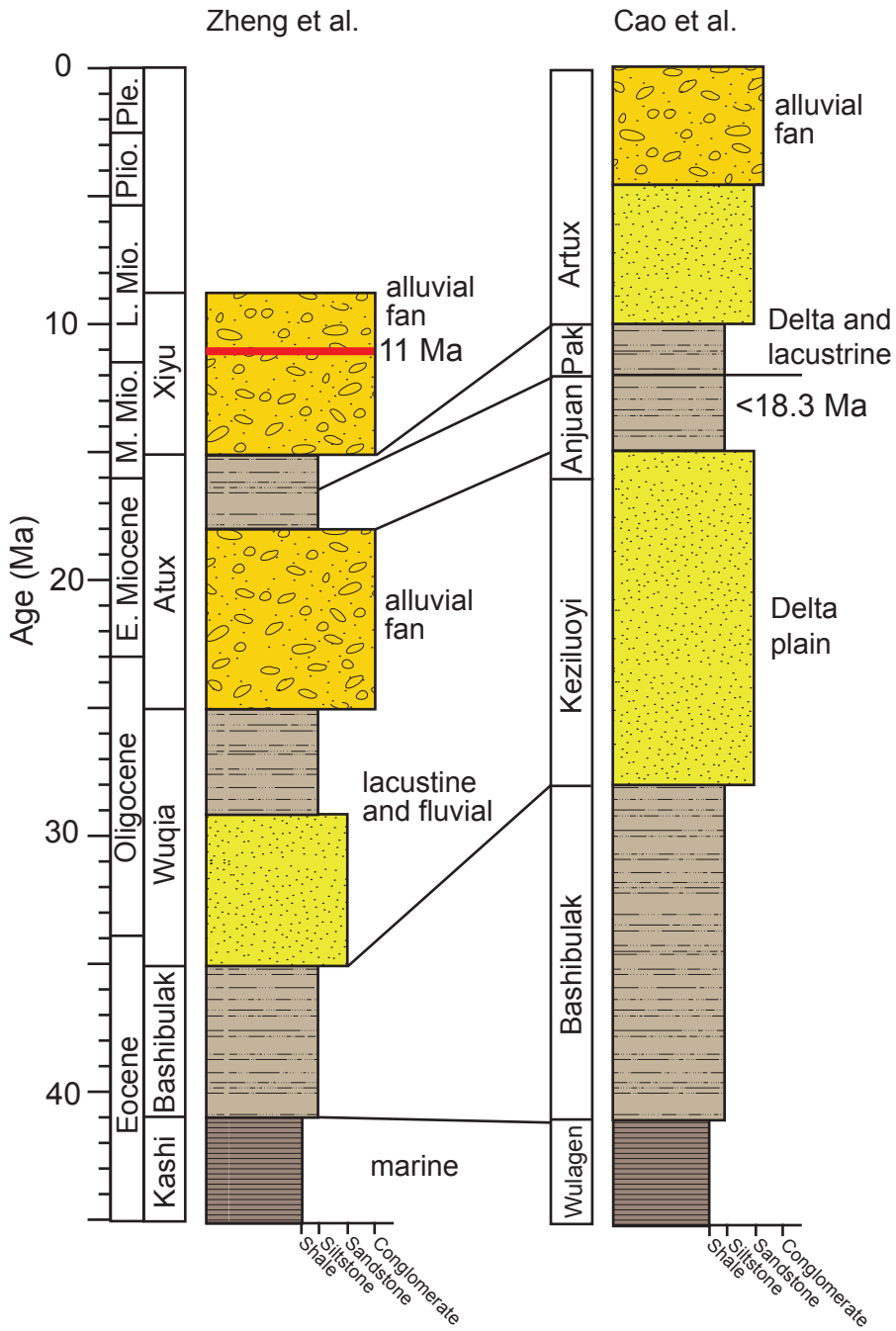

Figure 10
Clift et al,

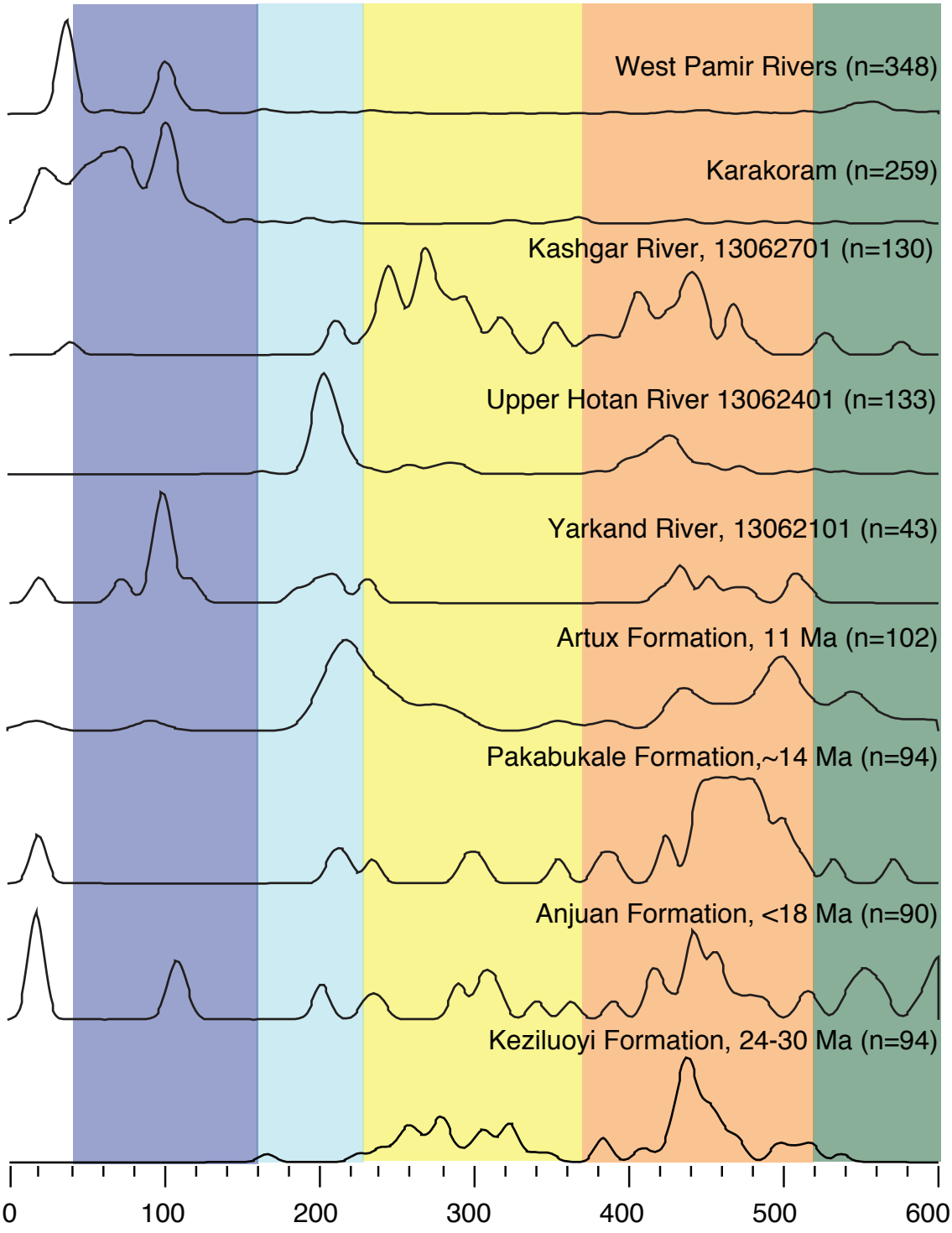

Figure 11
Clift et al.

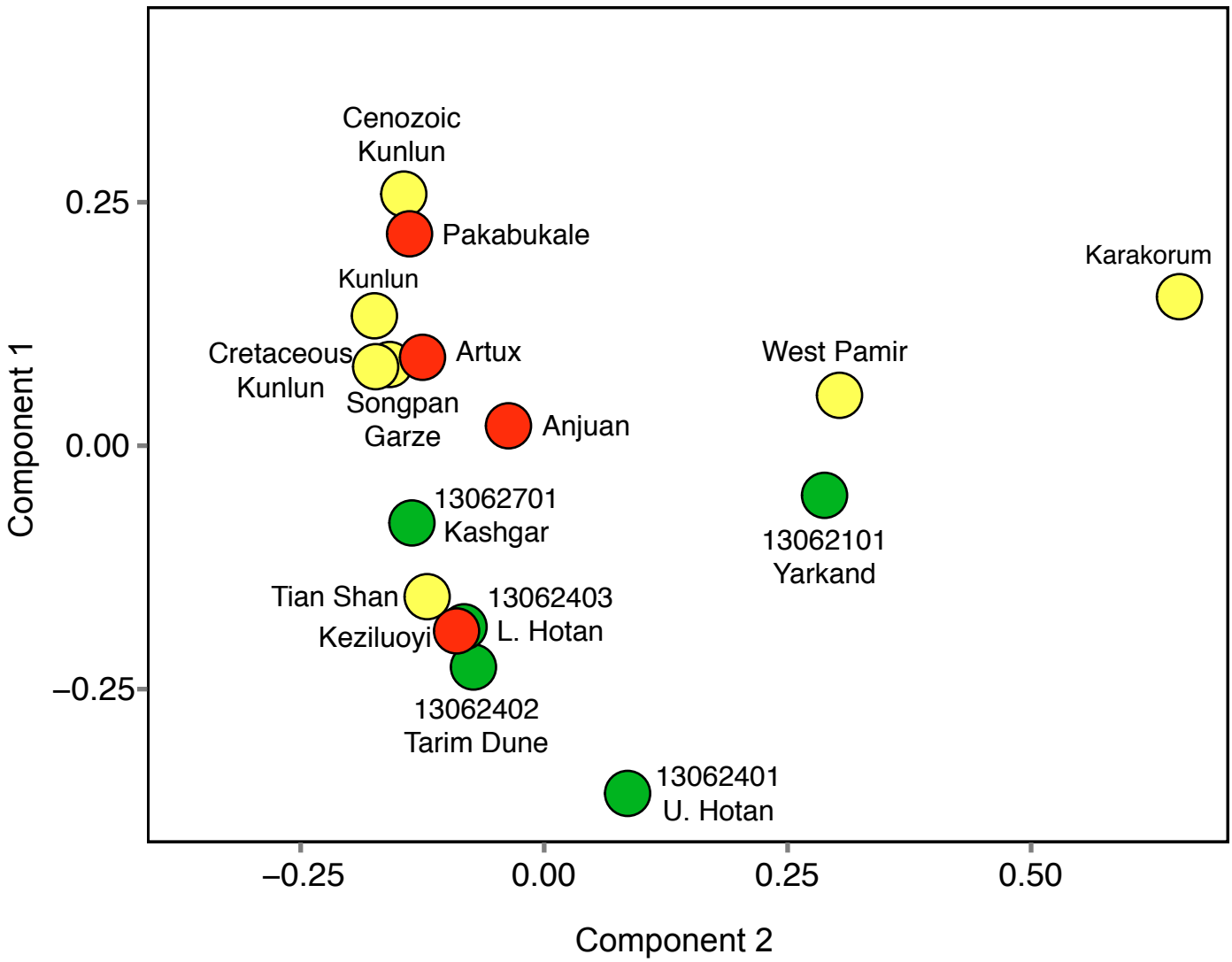

Figure 12
Clift et al.

Table 1

Sample Number	Location	Sample type	Latitude	Longitude
13062101	Yarkand River	Provenance	37° 56.32 N	76° 34.542 E
13062201	Kargilik River basin	OSL	37° 39.411 N	76° 49.454 E
13062202	Kargilik River basin	OSL	37° 39.411 N	76° 49.454 E
13062203	Kargilik River basin	OSL	37° 42.096 N	76° 51.670 E
13062401	Upper Hotan River	Provenance	37° 5.904 N	79° 57.596 E
13062402	Dune sand	Provenance	38° 27.229 N	80° 52.066 E
13062403	Lower Hotan River	Provenance	38° 27.229 N	80° 52.066 E
13062501	Mazatag Mounds	OSL	38° 37.074 N	80° 27.231 E
13062502	Mazatag Mounds	OSL	38° 37.112 N	80° 27.270 E
13062503	Dune sand	Provenance	38° 3’ 13.74” N	80° 12.164 E
13062701	Kashgar River	Provenance	39° 27.886 N	75° 52.513 E
13062703	Kashgar River	OSL	39° 27.886 N	75° 52.513 E

Table 2

Sample ID		SiO_2	TiO_2	Al_2O_3	Fe_2O_3	MnO	MgO	CaO	Na_2O	K_2O	P_2O_5	As	Ba	Ce	Co	Cr	Cu	Ga
13062101	Yarkand	64.4	0.33	11.3	2.54	0.045	1.91	7.73	2.56	2.35	0.1	5	509	52	6	28	12	13
13062401	Upper Hotan	69.9	0.49	12.2	3.25	0.079	1.57	3.88	2.57	2.7	0.17	14	354	77	7	51	10	15
13062402	Dune #2	67.6	0.41	10.6	2.66	0.053	1.84	6.63	2.43	2.2	0.1	5	535	51	7	43	10	10
13062403	Lower Hotan	66.7	0.50	11.0	3.07	0.061	1.98	6.64	2.49	2.32	0.15	6	456	62	8	54	12	13
13062701	Kashgar	69.7	0.39	7.3	2.74	0.056	1.25	7.97	1.69	1.22	0.08	5	382	39	6	34	13	7

		Mo	Ni	Nb	Pb	Rb	Sr	Th	Y	V	U	Zn	Zr	$^{87}Sr/^{86}Sr$	2σ SD	$^{143}Nd/^{144}Nd$	εNd	2σ SD
13062101	Yarkand	0	14	10	17	90	265	8	11	48	6	31	101	0.71427	0.000029	0.512086	-9.9	0.29
13062401	Upper Hotan	0	25	13	17	142	184	10	21	51	5	47	192	0.72196	0.000025	0.512175	-8.1	0.23
13062402	Dune #2	0	20	12	16	82	272	9	15	48	6	33	139	0.71843	0.000025	0.512084	-9.9	0.23
13062403	Lower Hotan	1	24	12	16	99	235	9	23	54	4	41	222	0.71996	0.000025	0.512102	-9.6	0.26
13062701	Kashgar	0	14	9	12	38	230	5	10	47	7	34	173	0.71172	0.000025	0.512158	-8.5	0.25

Table 3

Sample number	Location	Number of aliquots[1]	Depth (m)	U (ppm)	Th (ppm)	K (%)	Rb (ppm)	Cosmic (Gy/ka)[2]	Dose Rate (Gy/ka)[3]	Equivalent Dose, De (Gy)[4]	OSL Age (ka) ± 2se
13062201	Kargilik River	**19 (37)**	1.50	2.4 ± 1.7	10.5 ± 1.0	1.88 ± 0.05	96.6 ± 3.9	0.21 ± 0.02	3.26 ± 0.17	1.36 ± 0.61	**0.42 ± 0.19**
13062202	Kargilik River	**19 (45)**	2.00	2.6 ± 0.2	12.4 ± 1.1	1.75 ± 0.04	88.0 ± 3.5	0.20 ± 0.02	3.29 ± 0.18	8.47 ± 1.26[5]	**2.57 ± 0.46**
13062203	Kargilik River	**17 (47)**	1.00	2.2 ± 0.2	10.5 ± 1.0	1.70 ± 0.04	82.8 ± 3.3	0.23 ± 0.02	3.06 ± 0.16	4.27 ± 1.33	**1.40 ± 0.46**
13062501	Mazatag Mounds	**8 (43)**	2.50	2.2 ± 0.2	9.5 ± 0.9	1.66 ± 0.04	77.6 ± 3.1	0.17 ± 0.02	2.88 ± 0.16	1.44 ± 0.56[5]	**0.50 ± 0.20**
13062502	Mazatag Mounds	**13 (34)**	1.70	2.2 ± 0.2	10.3 ± 0.9	1.63 ± 0.04	76.3 ± 3.1	0.18 ± 0.02	2.93 ± 0.16	1.50 ± 0.49[6]	**0.51 ± 0.18**
13062703	Kashgar River	**26 (35)**	1.25	1.1 ± 0.1	4.5 ± 0.4	1.07 ± 0.03	44.9 ± 1.8	0.20 ± 0.02	1.74 ± 0.09	4.81 ± 2.11	**2.76 ± 1.24**

1 Number of aliquots used for age calculation, number of aliquots measured in parentheses. Rejection of aliquots follows standard rejection criteria. Samples analyzed following the single-aliquot regenerative-dose method (Murray and Winlte, 2000). See Supplemental data for more information.
2 Contribution of cosmic radiation to the dose rate was calculated by using sample depth, elevation, and longitude/latitude following Prescott and Hutton (1994).
3 Total dose-rate to quartz assumes 3±3%wt H_2O content of the sediments.
4 Equivalent dose (De) calculated using the minimum age model (MAM) of Galbraith and Roberts (2012) unless noted otherwise. Error on De is 2-sigma standard error.
5 De calculated using the central age model of Galbraith and Roberts (2012).
6 De calculated using the mean of the De data.